KTH ROYAL INSTITUTE
OF TECHNOLOGY

Doctoral Thesis in Fibre and Polymer Science

Design of Cellulose-Based Electrically Conductive Composites: Fundamentals, Modifications, and Scale-up

KARISHMA JAIN

Stockholm, Sweden 2022

Design of Cellulose-Based Electrically Conductive Composites: Fundamentals, Modifications, and Scale-up

KARISHMA JAIN

Academic Dissertation which, with due permission of the KTH Royal Institute of Technology, is submitted for public defence for the Degree of Doctor of Philosophy on Friday the 16th December 2022, at 2:00 p.m. in F3, Lindstedtsvägen 26, Stockholm.

Doctoral Thesis in Fibre and Polymer Science
KTH Royal Institute of Technology
Stockholm, Sweden 2022

ISBN 978-91-8040-405-1
TRITA-CBH-FOU-2022:55

Printed by: Universitetsservice US-AB, Sweden 2022

To the incremental progress of science.

Abstract

Modern demand for consumer electronics is fueling the generation of 'E-waste.' Furthermore, the raw materials and manufacturing methods used in the fabrication of electronics are not sustainable. There is therefore the need to develop renewable and sustainable raw materials for electronic devices that do not sacrifice performance; as well as a requirement to develop novel, scalable, sustainable electronic device fabrication methods that use these green electronic materials. To this end, bio-based materials are an environment-friendly alternative to non-renewable materials; and printed electronics could replace traditional manufacturing methods. Cellulose, one of the most abundant biopolymers on Earth, exhibits an interesting hierarchical structure. Due to extensive research over the years, there are a wide variety of established chemical modifications for cellulose, which can be harnessed to prepare high-performance electronic components. The hierarchical structure of cellulose is crucial in defining its material properties. In cellulose rich fibers, high molecular mass glucan polymers are commonly found in the form of cellulose nanofibrils (CNFs); these can be liberated and, once so, are capable of self-assembling into a wide variety of structures. Since cellulose is electrically insulating, it needs to be made into composites with conductive materials to form electrically conductive materials.

This thesis investigates the interaction between cellulose and the conductive polymer PEDOT:PSS (poly(3,4-ethylenedioxythiophene) : polystyrene sulfonate), and demonstrates how a fundamental understanding of the interactions between the two can be used to guide the chemical modification of cellulose for the large scale production of sustainable electronics. First, the PEDOT:PSS structure was studied using molecular dynamics (MD) simulations and experimental methods. Secondly, the interaction between cellulose and PEDOT:PSS was studied, and factors affecting this interaction were identified. This knowledge was then applied to propose a molecular interaction mechanism between these materials. Nanocellulose, especially cellulose nanofibrils (CNFs), have been integral to the development of bio-based conductive composites. However, the nanofibrillation process is expensive and energy-intensive. In addition, PEDOT:PSS is an expensive polymer. Therefore, in this work, chemically modified fibers were used to improve the interaction between cellulose and PEDOT:PSS; and prepare fiber-based bioelectronics and energy storage devices. The large-scale production of papers capable of energy storage has also been demonstrated using chemically-modified fibers, the factors affecting the processing of these materials have been identified throughout.

Keywords: Cellulose nanofibrils, PEDOT:PSS, chemically-modified cellulose fibers, fundamental interactions, bioelectronics, energy storage, conductive paper production, large-scale production.

Sammanfattning

En enorm efterfrågan på hemelektronik skapar ett stort "e-avfalls" problem i dagens samhälle. De råvaror som idag används för att tillverka elektronik har ett högt koldioxidavtryck, och traditionella tillverkningsmetoder för elektronik är dessutom energikrävande. Därför finns det en stort behov av högpresterande, hållbara, billiga, förnyelsebara råvaror för elektroniska komponenter. Dessutom behövs nya, hållbara bearbetningsmetoder för att producera elektroniska komponenter med lägre mängder inbyggd energi. I detta avseende är biobaserade material ett miljövänligt alternativ till icke-förnybara material och tryckt elektronik skulle kunna användas för att ersätta traditionella tillverkningsmetoder. Cellulosa är en mycket vanligt förekommande biopolymer i många växter och i vissa djur och det finns många rationella metoder för att utvinna denna polymer och polymeren är därför en mycket intressant råvara för framtida produkter. Den högmolekylära glukanmolekylen organiseras i i de flesta fallen i cellulosa nanofibriller (CNF) som sedan anordnas i en hierarkisk struktur i makroskopiska fibrer. Modern forskning har också visat att de frilagda fibrillerna kan självorganiseras i skräddarsydda nano-strukturer som kan vara mycket intressanta för att tillverka högpresterande elektroniska komponenter. Med hjälp av all den forskning som genomförts för cellulosamaterial genom åren finns det också tillgång till en fantastisk verktygslåda för att kemiskt modifiera cellulosa för att passa i olika tillämpningar. Eftersom cellulosa är elektriskt isolerande är det nödvändigt att kombinera cellulosa med ett ledande material för att skapa skräddarsydda komponenter med god elektrisk ledningsförmåga.

Arbetet i denna avhandling har fokuserats på studera växelverkan mellan cellulosa och den ledande polymer PEDOT:PSS, och för att klarlägga hur denna grundläggande förståelse kan utnyttjas för att identifiera nödvändiga kemiska modifieringar på cellulosan för att överföra resultaten till storskalig produktion av hållbar elektronik. Initialt studerades den molekylära och övermolekylära strukturen hos PEDOT:PSS komplex med en kombination av molekylärdynamiska (MD) simuleringar och experimentella undersökningar. För det andra studerades växelverkan mellan cellulosa och PEDOT:PSS, och det visade sig möjligt att identifiera de faktorer som kontrollerar denna växelverkan. Dessa kunskaper användes sedan för att molekylärt förklara hur dessa material fundamentalt växelverkar med varandra. Nanocellulosa, särskilt cellulosa nanofibriller (CNF) har varit en del av biobaserade ledande kompositer. Nanofibrilleringsprocessen är dock kostnads- och energikrävande. Dessutom är PEDOT:PSS en dyr polymer. Därför användes i detta arbete kemiskt modifierade fibrer för att förbättra interaktionen mellan cellulosa och PEDOT:PSS (för att minska kostnaderna), och för att förbereda fiberbaserad bioelektronik och energilagringsenheter. Storskalig produktion av energilagringspapper demonstrerades också med kemiskt modifierade fibrer och faktorer som påverkar bearbetningen av dessa material identifierades.

List of Appended Papers

This thesis is a summary of the following appended papers:

Paper I

PEDOT:PSS Nano-Particles in Aqueous Media: A Comparative Experimental and Molecular Dynamics Study of Particle Size, Morphology and z-Potential
Karishma Jain, Aleksander Mehandzhiyski, Igor Zozoulenko, Lars Wågberg
Journal of Colloid and Interface Science 2021, *584*, 57

Paper II

On the Interaction Between PEDOT:PSS and Cellulose: Adsorption Mechanisms and Controlling Factors
Karishma Jain, Michael S. Reid, Per A. Larsson, Lars Wågberg
Carbohydrate Polymers 2021, *260*, 117818

Paper III

3D printable composites of modified cellulose fibers and conducting polymer and their use in wearable electronics
Karishma Jain, Zhen Wang, Leonardo D. Garma, Emile Engel, Göksu Cinar Ciftci, Cecilia Fager, Per A. Larsson, Lars Wågberg
Manuscript

Paper IV

Role of Dialcohol-modified cellulose fibers in improving structure and performance of PEDOT:PSS
Karishma Jain, Emile Engel, Michael S. Reid, Per A. Larsson, Lars Wågberg
Manuscript

Paper V

Production of Energy-Storage Paper Electrodes Using a Pilot-Scale Paper Machine
Patrik Isacsson, Karishma Jain, Andreas Fall, Valerie Chauve, Alireza Hajian, Hjalmar Granberg, Lucie Boiron, Magnus Berggren, Karl Håkansson, Jesper Edberg, Isak Engquist, Lars Wågberg
Journal of Materials Chemistry A 2022

Contributions to the Papers

The author's contribution to the appended papers is as follows:

Paper I. First author. Did all the laboratory work. Equally shared planning and data analysis with other authors. Contributed equally to the preparation and editing of the manuscript.

Paper II. First author. Most of the planning, experimentation, and data analysis. Prepared the manuscript.

Paper III. First author. Most of the planning, experimentation, and data analysis. Prepared the manuscript.

Paper IV. First author. Most of the planning, experimentation, and data analysis. Prepared the manuscript.

Paper V. Second author. Contributed to the planning, experimentation, and data analysis. Contributed to the preparation of the manuscript.

Related Work

Papers not included in this thesis:

Paper I

Nanocellulose and PEDOT:PSS composites and their applications
Robert Brooke, Makara Lay, Karishma Jain, Hugo Francon, Mehmet Girayhan Say, Dagmawi Belaineh, Xin Wang, Karl M. O. Håkansson, Lars Wågberg, Isak Engquist, Jesper Edberg & Magnus Berggren
Polymer Reviews 2022, 1-41

Paper II

Digital Cellulose – Recent advances in electroactive paper
Robert Brooke, Karishma Jain, Patrik Isacsson, Andreas Fall, Isak Engquist, Valerio Beni, Lars Wågberg, Hjalmar Granberg, Ursula Hass, Jesper Edberg
Submitted Manuscript

Paper III

Multifunctional composite paper adaptable to industrial papermaking
Alireza Hajian[1], Karishma Jain[1], Chandrashekhar Subramaniyam, Lars Wågberg, Mahiar Max Hamedi
Manuscript

Paper IV

Elucidating the Fine-scale Structural Morphology of Nanocellulose by Nano Infrared Spectroscopy
Magnus Johnson, Nikolay Kotov, Per Larsson, Karishma Jain, Lars Wågberg, Tiffany Abitbol, Adrian Cernescu
Carbohydrate Polymers 2022

Patent

Conductive composition comprising dialcohol-modified cellulose and uses Thereof
Karishma Jain, Lars Wågberg, Per A. Larsson, Hjalmar Granberg
P6334SE00

Abbreviations

AFM	Atomic force microscopy
AGU	Anhydroglucose unit
CMC	Carboxymethyl cellulose
CM-CNFs	Carboxymethlyated cellulose nanofibrils
CNF	Cellulose nanofibril
DALC	Dialcohol-modified cellulose
DM	Degree of modification
EDS	Energy dispersive x-ray spectroscopy
FIB	Focused ion-beam
GTMAC	Glycidyltrimethylammonium chloride
PEDOT	Poly(3,4-ethylenedioxy thiophene)
PSS	Poly (styrene sulfonate)
QCM-D	Quartz crystal microbalance with dissipation
SEM	Scanning electron microscopy
TEMPO	2,2,6,6-tetramethylpiperidine 1-oxyl
TGA	Thermogravimetric analysis
WAXS	Wide angle x-ray scattering
XPS	X-ray photoelectron spectroscopy

Contents

1. Introduction

1.1. Context

Since the invention of conductive polymers, the field of organic electronics has grown exponentially. Conductive polymers have enabled the solution-based fabrication of electrodes at room temperature. The resulting materials have good electrical and ionic conductivities, and can be cheaply printed on an industrial scale. This has given rise to a new interdisciplinary field of bioelectronics. Conventional silicon devices cannot conduct ions and are mechanically rigid; however printed electronics are predominantly plastics so do not have these limitations. For energy storage applications, it is desirable to have electrodes with 3D porous geometries and high specific surface areas, hence printed electronics are ideally suited for such applications.

The ubiquitous substrate for information transfer (writing, printing, packaging, etc.) has for long been *paper,* which consists of the most used bio-based material, *cellulose*. The paper-making process was developed in China in the early second century. Since then, the production of paper and its applications have increased exponentially. Paper is an attractive choice of substrate for electronics due to its flexibility, porosity, environmental friendliness, cost-effectiveness, and the existence of a well-developed paper industry. In addition, there exists a well-developed printing industry, with high-resolution printers capable of printing on a vast range of substrates. The discovery of conductive polymers and organic electronics have revolutionized the printing industry and have led to the invention of *printed electronics*. Cellulose fibers are increasingly seen as a *sustainable* substrate for printed electronics. However, cellulose fibers have the potential to be more than just a substrate. The chemical modification of cellulose fibers allows the tailoring of their mechanical properties to different applications. In order to harness the potential of cellulose in organic and printed electronics, a fundamental understanding of the interaction between cellulose and conducting polymers is important.

The escalating problem of electronic waste, so-called “E-waste”, in the 21st century is a growing concern given its negative impact on the environment. Heavy metals

and toxic chemicals from discarded electronic devices leach into the environment where they can contaminate water and soil. Toxic and non-renewable raw materials should be designed out of future electronics to alleviate this issue. Thus, research and innovations in cellulose-based electronics are crucial to achieve *sustainable electronics*.

1.2. Thesis Objectives

The objectives of this work are:

1. To understand the structure and chemistry of PEDOT:PSS polymer and its interactions with cellulose.
2. Identify the chemical modifications of cellulose that improve the interactions with PEDOT:PSS.
3. Demonstrate the large-scale production of bio-based electrodes for energy storage applications.

Sustainable and Green Electronics are not only needed to address the 'E-waste' problem, but also to combat climate change. The United Nations have listed 17 Sustainable Development Goals (SDGs) to combat the problems of fossil-based materials and increase sustainable behavior in our daily lives. In this regard, wood-based materials can help mitigate the issues associated with fossil-fuel derived plastics. This work attempts to increase the sustainability of everyday electronic devices while addressing the UN´s SDGs, specifically: good health and well-being (SDG 3), clean and affordable energy (SDG 7), industry, innovation, and infrastructure (SDG 9), responsible consumption and production (SDG 12), climate action (SDG 13), and partnerships for goals (SDG 17), to combat climate change. Overall, it attempts to take an incremental step toward an innovative circular electronics industry.

2. Background

This section aims to provide the relevant background for a clear understanding of the research results described in this thesis.

2.1. Wood fibers and components

Wood has a 3D hierarchical structure consisting of long, highly anisotropic, slender fibers; which provide mechanical strength and durability to trees. Chemically, wood fibers are composed of three main constituents: cellulose (40-50%), hemicellulose (25-35%) and lignin (25-35%). Additionally, there is also a small fraction of "extractives". The wood tissue has a layered structure, consisting of: a lignin-rich middle lamella and a hemicellulose-rich primary layer that helps to hold the cellulose fibers together; three secondary layers (S1, S2, S3), rich in cellulose and hemicellulose with small amounts of lignin, these secondary layers provide the mechanical strength; and a cell lumen which is used to transport water and nutrients. The cellulose fibers are liberated from wood fibers by chemical and/or mechanical treatment (called pulping). In these processes the chemical treatment removes most of the lignin and some hemicellulose, while mechanical pulping methods typically have much higher yields of the fibrous components. The products of the chemical treatment are commonly called "pulp fibers".[1]

2.1.1. Hierarchical structure of cellulose

Cellulose is among the most abundant renewable biopolymers on Earth. It is a linear polysaccharide of β-1,4 linked D-glucopyranose, also called "anhydroglucose" units (AGU), (Figure 1). Cellulose chains are assembled into high-aspect ratio, semicrystalline cellulose nanofibrils (CNFs) *via* van der Waals interactions as well as inter- and intra-molecular hydrogen bonds. These fibrils strongly associate with one another to form fibril aggregates in the fiber wall. The fibril aggregates form hollow fibers that are typically 20–40 μm wide, with a fiber-wall thickness of approximately 5 μm and a length of a few millimeters.[2,3]

There are two technically relevant crystal structures of cellulose. The native cellulose polymer is called cellulose I, where all the cellulose chains run in the same direction (parallel). However, after dissolution and regeneration of cellulose I, a

more thermodynamically stable crystallographic structure, cellulose II, can be formed, where chains are present in an antiparallel orientation.[4,5] There are many different solvent systems that can be used for the dissolution of cellulose. This thesis uses cellulose model surfaces prepared from the dissolution of cellulose in the NMMO/DMSO solvent system, which produces semicrystalline regenerated cellulose II surfaces.[6]

2.1.2. Nanocellulose

CNFs consist of ordered cellulose molecules which makes them very stiff, with a Young's modulus of 130–150 GPa, which is comparable with many metals, alloys, and polymers.[7–10] Individual CNFs can be liberated from the cellulose fiber cell wall. The preparation of micro-fibrillated cellulose (MFC) was first demonstrated by Turback et al., using the high-pressure homogenization of wood pulp fibers.[11,12] However, this is an energy-intensive process and, for that reason, was never commercialized. Instead, research was conducted to find less energy intensive fibrillation processes. Approaches whereby the fibers are pretreated by physical beating, enzymatic or chemical methods, were investigated. The chemical pretreatments focused on introducing charges in the fiber wall to help liberate CNFs and reduced the energy required for fibrillation.[13–15] The high surface area, good rheological properties, potential for surface functionalization, unique colloidal properties, and high aspect ratio of CNFs have led to the development of a multitude of functional composites.[2,15,16] Another class of nanocellulose obtained from wood is cellulose nanocrystals (CNCs). These are highly crystalline, stiff, short, rod-like nanoparticles (520 nm wide and 50-350 nm long) prepared by the acid hydrolysis of cellulose pulp fibers. CNCs produced from sulfuric acid treatment are colloidally stable and can self-assemble to form chiral, nematic structures that can be utilized in different engineering and biomedical applications.[17,18]

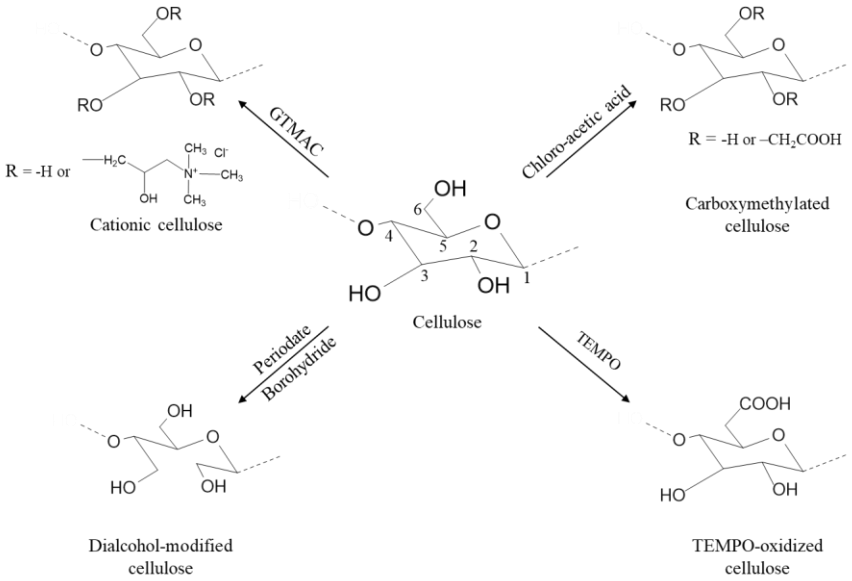

Figure 1 The chemical structure of native cellulose and the chemical treatments required for the different chemical modifications of cellulose used in this work. TEMPO: 2,2,6,6-tetramethylpiperidine 1-oxyl, GTMAC: glycidyltrimethylammonium chloride.

2.2. Chemical modifications of cellulose

Native cellulose is highly ordered, insoluble in water, stiff, and difficult to process and is lacking a glass transition temperature (as it starts to thermally degrade). The presence of a primary hydroxyl at C6 and secondary hydroxyls at the C2 and C3 positions (Figure 1), provide a route by which the cellulose can be chemically modified to tailor its interactions with other materials and thereby form composites.[19,20] In addition, these modifications often act as a pretreatment to reduce the energy consumption of mechanical fibrillation of the cellulose fibers into CNFs. Over the years, different chemical modifications of cellulose have been proposed.[19] This thesis is limited to simple, aqueous-based chemical modifications; the focus being to study and optimize the interactions of cellulose with PEDOT:PSS. The chemical modification investigated are: carboxymethylation, TEMPO-oxidation, periodate oxidation with subsequent borohydride reduction, and cationization (Figure 1). This section provides a brief description of each of these

modifications. For the detailed reaction procedures, the reader is directed to the appended articles.

2.2.1. Carboxymethylation (Paper II)

As the name implies, carboxymethylation is used to introduce acetic acid groups onto the primary and secondary hydroxyls of AGU in cellulose, by chemical treatment of the pulp fibers using monochloroacetic acid.[21,22] The degree of substitution can be determined by controlling the reaction conditions. Carboxymethyl CNFs (CM-CNF) with a charge density of 600 μeq/g were used in this work and provided by RISE Bioeconomy.

2.2.2. TEMPO-mediated oxidation (Paper II)

Another way to introduce carboxyl groups to the cellulose backbone is *via* the TEMPO-mediated oxidation of the cellulose fibers. TEMPO-mediated oxidation is highly specific, pH-sensitive, and can selectively modify only the C6 hydroxyl groups.[13,14,23,24] The reaction can be carried out at alkaline or neutral pHs. However, the alkaline conditions have been observed to degrade cellulose chains, leave residual aldehydes and lead to lower degrees of cellulose polymerization. In this work, a method developed by Saito et al. was used to prepare carboxylated cellulose fibers with a charge density of 600 μeq/g by TEMPO-mediated oxidation at pH 6 (to preserve the molecular mass of the cellulose).[13]

2.2.3. Periodate oxidation and borohydride reduction (Paper III-IV)

Periodate oxidation is routinely used to oxidize the 1,2-dihydroxyls to dialdehydes for structural analysis of carbohydrates. The periodate oxidation cleaves the C2-C3 bond in cellulose and introduces two aldehyde groups, after which the polymer is termed dialdehyde cellulose.[25,26] These dialdehyde groups can be further converted to different functional groups, such as carboxylic acids or primary alcohols. One such reaction is the reduction of dialdehyde cellulose to dialcohol cellulose (DALC), commonly performed by using sodium borohydride as the reducing agent. DALC cellulose displays thermoplastic behavior and can therefore, unlike native cellulose, be melt-processed. As a result of this, DALC fibers have been used in applications like transparent packaging materials.[27–30] For this thesis, DALC fibers with

different charge densities were prepared using sequential periodate oxidation and borohydride reduction steps, using the same reaction conditions as described earlier by Larsson et al.[28]

2.2.4. Cationic modification of cellulose (Paper V)

Positive charges can be introduced into cellulose by functionalizing with amines. An example of one such process is the addition of surface quaternary ammonium groups, which are charged over the entire pH scale. The reaction conditions are similar to those used for preparing cationic starch in the paper industry.[31] This directly converts the cellulose hydroxyl groups to quaternary ammonium groups by reacting with glycidyl-trimethylammonium chloride (GTMAC) under highly alkaline conditions.[32] A charge density of 300 μeq/g was prepared for this work. However, different charge densities of cationic quarternary ammonium groups can be obtained by changing the GTMAC:cellulose ratio.

2.3. Electrically conductive materials

With the advent of organic electronics, conjugated polymers and carbon-based materials became the focus of intense research due to their ability to be processed in aqueous solutions as well as their excellent electrical, electrochemical, and mechanical properties. This section aims to provide the reader with background information about these materials.

2.3.1. Conducting polymers

The first conducting polymers (CPs) were reported in 1977, with the synthesis and characterization of halogen-doped-polyacetylene.[33,34] The development of CPs was awarded the Nobel prize in 2000. In CPs, alternating single and double bonds form a conjugated system between sp^2-hybridized carbon atoms. The three sp^2 orbitals form strong σ-bonds, and the fourth P_z orbital forms a π-bond between neighboring carbon atoms. These π-orbitals lead to the formation of bonding (π) and antibonding (π^*) orbitals. As the number of combined orbitals increase they form bands and band gaps. The valence band (π) is defined as highest occupied

molecular orbital (HOMO) and conduction band (π^*) is defined as lowest unoccupied molecular orbital (LUMO).[35,36]

Pristine CPs have an unfilled conduction band, hence a low conductivity. The conductivity can be increased by chemical or electrochemical doping. Therefore, the conductivity range of pristine CPs span from insulators to semiconductors. Both electron accepting (p-type) and electron donating (n-type) doping can be used to make CPs conductive. A detailed explanation of charge transport in CPs is beyond the scope of the work and can be found elsewhere.[37] Some early examples of highly conductive polymers are doped polyacetylene, polyaniline (PANI), and polypyrrole (PPy).[35] However, the use of these polymers was limited because they suffered from instability in air, poor processability, opacity, and would degrade to form hazardous compounds on degradation (in the cases of PANI and PPy). In 1988, researchers at Bayer (Jonas, Heywang, and Schmidtberg) synthesized the highly conductive and air stable polymer PEDOT (Figure 2a) by oxidative polymerization in the presence of PSS (Figure 2b). Soon after, the discovery of PEDOT:PSS, where PEDOT is polymerized *in situ* with PSS as a counterion, by researchers at Agfa, revolutionized the field of conductive polymers and organic electronics. Doped CPs have good electrochemical properties, are air stable and highly conductive. As such doped CPs have been used in various applications like sensors, displays, energy storage, energy harvesting and energy generation, to name but a few.[38–41]

2.3.2. PEDOT:PSS

After the invention of water-based PEDOT:PSS dispersions, the scientific interest in conducting polymers has grown rapidly. PEDOT:PSS is a water-dispersible form of PEDOT where PSS (which is not conductive) is used as a counterion in order to facilitate solvation, to balance charges, and create polyelectrolyte complexes of PEDOT and PSS.[42] The other commonly used counterion for PEDOT is tosylate (toluene-4 sulfonate), which behaves similarly to PSS but lowers the water dispersibility.[43] PEDOT:PSS is a stable, p-doped conductor with excellent optical and electrochemical properties; which has led to it having great commercial success.[38,44] The conductivity of PEDOT:PSS can range between 10^{-1} S/cm to 10^{3} S/cm. The conductivity is dependent on the π-π stacking of PEDOT chains and the

crystallinity of the polymer, which is determined by the synthesis method, level of doping, counterion type, and post-processing methods.[45,46]

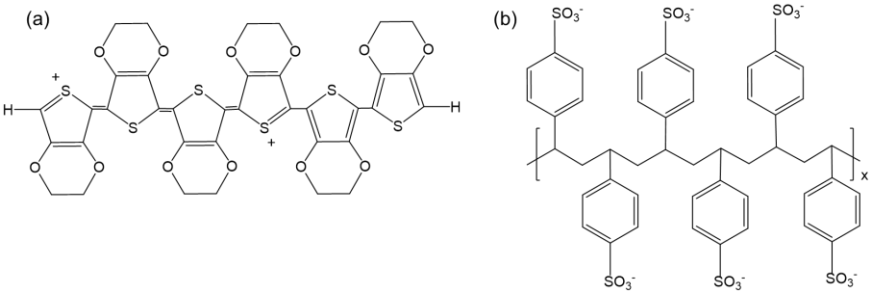

Figure 2 The chemical structures of (a) poly (3,4-ethylene dioxythiophene), PEDOT; and (b) poly(styrene sulfonate), PSS.

PEDOT:PSS is a polyelectrolyte complex with a core-shell morphology, where a hydrophobic, conductive PEDOT core is surrounded by PSS.[47] This structure limits the charge transport in pristine PEDOT:PSS films since the conducting PEDOT domains are separated by insulating PSS polymer chains. Therefore, several strategies have been developed to increase the charge transport by altering the stacking of PEDOT in PEDOT:PSS films.[48–50] One such method is secondary doping with organic solvents, acids, salts, or ionic liquids.[51–55] These dopants work by bringing PEDOT chains closer together and increasing the PEDOT crystallinity while removing excess PSS and PSS aggregates.

In addition to electronic conductivity, CPs also allow ionic conduction. This combination of being ion and electron conductive broadens their applicability. Due to its high conductivity, ion conduction, and electrochemical stability, PEDOT:PSS is widely used to create pseudocapacitors, electrochromic displays, and electrochemical transistors.[53,56]

2.4. Electrochemical energy storage

There are many forms of energy storage, (e.g. kinetic, thermal, chemical, electrochemical, etc.). The energy storage devices that have revolutionized consumer electronics, green mobility, and continuous power supply are batteries and supercapacitors. These devices typically consist of two electrodes (made up of active materials like carbon, conducting polymers, and 2D materials) separated by

an electrolyte. Paper-based electrodes can alleviate several challenges currently faced in fabricating high-performance electrodes, described in Section 2.5.[57]
The following section will explain the basics of supercapacitors and their characterization methods.

2.4.1. Supercapacitors

Capacitors are the fundamental energy-storage components in both analog and digital electronics. Although capacitors can be fabricated in different geometries, conventional parallel plate capacitors consist of two parallel conductors (typically metal plates) separated by an insulator with a high dielectric constant. The energy is stored in the electric field between two oppositely charged conductors. The ability to store energy in the form of charge is defined as a capacitance (C), which is the ratio of the amount of charge (Q) that can be stored at an applied voltage (V) as given in Eq. 1.

$$C = Q/V = \varepsilon A/d \qquad \text{(Eq. 1)}$$

where A is the area of the plates, d is the separation between them, and ε is the dielectric permittivity of the material between the plates.
In supercapacitors, the dielectric between the two conductors is an electrolyte (ion conductor). Based on the charge storage mechanism, supercapacitors can be divided into electric double-layer capacitors (EDLC) and pseudocapacitors. In EDLC, the mobile ions in the electrolyte migrate to the charged metal plates when a potential is applied across them. This leads to the build-up of the electric double layer (EDL) of counterions at the electrode surface. The EDL consists of three layers: the inner Helmholtz plane (IHP) containing solvent molecules and counterions, the outer Helmholtz plane (OHP) with solvated ions, and the diffuse layer that extends out into the bulk electrolyte. The IHP is directly in contact with the electrode surface and only a few angstroms thick. Since the distance between two oppositely charged layers is so small, the capacitance of EDLCs is much higher than that of a conventional, solid dielectric, capacitors. Most commercial EDLCs use carbon as an electrode.
Pseudocapacitors rely on electrochemical reactions (such as ion intercalation or redox reactions) to store chemical energy when a voltage is applied. Hence, the working principle of a pseudocapacitor is more like a battery. Both EDLC and

pseudocapacitors depend on the movement of ions throughout the electrode. CPs, such as PEDOT, PANI, or PPy, are more suited for pseudocapacitor fabrication, because of their mixed ion-electron conduction and ability to undergo redox reactions.[58] There are also hybrid capacitors where both EDLC and pseudocapacitors principles are combined. These are fabricated with one carbon-based electrode and one conductive polymer electrode, thereby combining two charge storage mechanisms, which has been shown to lead to higher capacitances.[59]

2.4.2. Electrochemical characterization methods

Electrochemistry studies the correlation between chemical reactions and electric currents. Electrochemical cells are used for electrochemical characterization, and consists of at least two electrodes separated by an electrolyte. Typically, new electrode materials are characterized in a three-electrode system. The three electrodes are: (1) The reference electrode (*RE*), this has a known and constant potential to which the potentials of other electrodes are compared. Some examples are Ag/AgCl and the standard hydrogen electrode (SHE); (2) The working electrode (*WE*), which is the electrode under investigation; (3) The counter electrode (*CE*), which is used to supply the counter charge to the WE. A platinum mesh or wire can be used as a RE due to its low reactivity in organic or aqueous electrolytes. A potentiostat, the equipment used to apply and monitor the potential change at the electrodes, is connected to the electrodes.

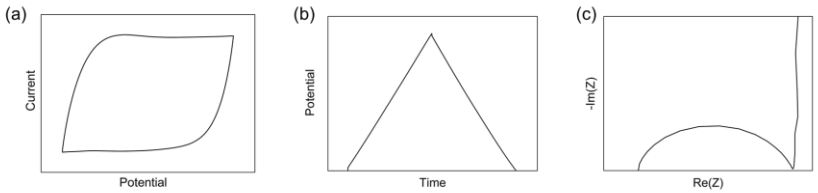

Figure 3 A schematic illustration of typical (a) cyclic voltammetry plot, (b) galvanostatic charge-discharge plot, and (c) Nyquist plot for a pseudocapacitor.

***Cyclic Voltammetry*:** Cyclic voltammetry (CV) is a potential sweep method where the current change at the WE is monitored while the voltage is cycled at a constant scan rate (voltage/time). A voltammogram or CV curve gives information

about the electrochemical system and the nature of electrochemical reactions in the system (faradaic and non-faradaic). For example, a pseudocapacitor or EDLC shows a square voltammogram (Figure 3a) indicative of capacitive charging and no redox reaction. The capacitance of the system can be calculated from the CV curve as follows:

$$I = C\,(dV/dt) \qquad \text{(Eq. 2)}$$

where I is the current at the WE, C is the capacitance, and dV/dt is the scan rate.

***Chronopotentiometery*:** Chronopotentiometery, or galvanostatic charge-discharge (GCD), is the electrochemical method where the change in potential of the WE is monitored over time at a constant current. A typical GCD curve for a capacitive charge-discharge process (Figure 3b) exhibits a linear increase and decrease in potential during charge-discharge cycles. GCD measurements are often used to quantify the capacity, energy and power density of a supercapacitor. In addition, the cycling stability can also be tested with this method. The capacitance quantification from GCD measurements is more accurate than those obtained by CV; as it is done at a constant current, which better emulates real-world devices. The capacitance is calculated from the slope of the V-t curve (dV/dt) using Eq.2.

***Electrochemical Impedance Spectroscopy (EIS)*:** This method characterizes the system's impedance over a range of frequencies using an applied AC voltage. EIS is used to investigate the different physical and chemical processes in electrochemical cells at different timescales, which is why spectra are collected across a range of frequencies. The impedance data are conventionally analyzed by plotting in a “Nyquist plot”, i.e. plotting the real and imaginary parts of the impedance measured at different frequencies. The information for each physical and chemical process can be obtained by fitting the data to an equivalent circuit. A typical EIS spectrum for a supercapacitor is shown in Figure 3c. It consists of a semi-circle at high frequencies, and a vertical straight line at low frequencies. The semi-circle represents the internal resistance (electrolyte + charge transfer resistance), and the straight line can be related to the electrode's diffusion process.[60]

2.5. Cellulose-based conducting composites

Cellulose is an abundant, versatile, sustainable and inexpensive material; used as a flexible substrate in paper based electronics.[61] Although cellulose is naturally insulating, there is a growing interest in using cellulose in electronic devices, especially as electrodes in electrochemical energy storage devices and Medtech applications. There are several reasons for this: (i) it is mechanically flexible, light-weight, and strong (especially CNFs); (ii) The tunable properties like porosity and pore-size distribution of cellulose-based materials provides good ion permeability and selectivity; this makes them suitable for many applications, such as separators in batteries or fuel cells; (iii) The surface hydroxyl groups of cellulose provide a route to chemical and/or physical modification, which makes cellulose suited to act as a binder in electrode materials; (iv) The dispersive nature of CNFs (it can disperse conductive materials that are not themselves easily dispersed in aqueous solutions), as well as its colloidal stability, can be used to create aqueous conductive inks; (v) The large surface area of cellulose is ideal for increasing material loading as well as the active area of electrodes; (vi) The biocompatibility, biodegradability and environmentally friendly nature of cellulose means that it can be used to make recyclable electrodes and makes it suited *to in* vivo bioelectronic applications; (vii) An established paper making industry already exists, making the scale up of manufacturing easy and negating many startup capital costs and should allow a faster time to market.[57,62] Although there are many ways to make cellulose conductive, such as carbonization, this work is limited to the use of cellulose and conductive polymers/carbon composites.

Conductive coatings on flexible substrates have a thickness limitation to avoid cracking during bending. The substrate is the major component of the device weight and has no active role in charge transport. This is especially problematic for electrodes in energy storage devices, where light-weight, 3D morphologies, and high active material loadings are crucial to improving performance.[57] One solution is CNFs functionalized with conductive materials. CNFs can be used as templates that increase the mass-loading by interacting with conductive materials. The 3D structure of CNFs is retained when combined with conductive nanomaterials, this porous 3D network increases the active surface area of the electrodes, which is

better for charge and ion transfer. Likewise, the CNF adds structural support to the electrodes. The conductive materials most commonly used with cellulose are carbon (in the form of carbon nanotubes (CNTs), graphite, and carbon black) and conducting polymers due to their high electronic conductivity, redox activity, and ion-intercalation ability.

2.5.1. CNF and conducting polymer composites

CPs and cellulose composites can be prepared either by the *in situ* polymerization of a CP on cellulose or by blending.[63] For PPy and PANI, *in situ* polymerization is often used to obtain free-standing electrodes, since they are insoluble and unstable in water.[64–71] This method has been used to create uniform, highly conductive, redox-active coatings on cellulose fibers/fibrils. The excellent performance of these composites is attributed to the favorable interactions between surface functional groups of cellulose and the –NH or –N groups of PPy and PANI. It has also been shown that the type of pulp and the chemical nature of the cellulose (carboxymethyl cellulose (CMC) or CNFs) can affect the polymerization yield, mechanical properties, and conductivity of the CP/cellulose composites.[72,73]

PEDOT:PSS and nanocellulose composites have been very popular for decades. Several fabrication methods have been developed for these composites, such as: layer-by-layer assembly of polyelectrolytes and PEDOT:PSS on wood-sourced fibers,[74–76] mixing microfibrillated cellulose (MFC)[77,78] or CNFs[79–82] with PEDOT:PSS. The colloidal properties of nanocellulose also provide an added advantage when making PEDOT:PSS inks.[82,83] Since nanocellulose is insulating, an excess PEDOT:PSS and additives are required to increase the conductivity of PEDOT:PSS composites.

Most of the research into CNF/PEDOT:PSS composites is focused on characterizing the resultant material properties, rather than understanding them on a fundamental level. It is important to understand the molecular interactions within the material in order to tune the final material's properties.[84] To the best of the author´s knowledge, there are only a few studies that focus on optimizing the interaction between cellulose and PEDOT:PSS. Montibon et al.[77] studied the effect of pH and salt concentration on the interactions between PEDOT:PSS and MFC. The effect of different types of cellulose (CMC and CNFs) on the conductivity of

cellulose/PEDOT:PSS composites was also studied experimentally and computationally.[81,85] It was found that anisotropic (i.e., high aspect ratio) CNFs provide a better charge transport in the composite nanopaper than, isotropic, CMC composites.

Furthermore, van der Waals interactions, H-bonding, or hydrophobic interactions have repeatedly been used to describe the interactions between PEDOT:PSS and CNFs.[79,80,86] This thesis elaborates on the interaction model between PEDOT:PSS and cellulose, and presents strategies to modify cellulose to improve its interaction with PEDOT:PSS.

2.5.2. CNF and carbon composites

Carbon materials such as graphite, carbon black, or activated carbon have been widely used as cheap, abundant and porous electrode materials. Different 1D and 2D carbon materials such as CNTs and graphene have been used with CNF to form conductive composites. Carbon based materials are generally hydrophobic and require chemical treatments to be well-dispersed in water. It has been shown that CM-CNFs or TEMPO-oxidized CNFs can disperse CNTs and other carbon materials such as graphite or graphene without surfactants.[87–89] The reason for this is the high dispersive energy of CNFs, as well as the electrostatic repulsion between negatively charged CNFs and carbon materials (which typically carry a net negative charge). Another reason is the entropic gain due to the release of water molecules when CNT adsorbs onto CNF, this process is loosely defined by many investigators as “hydrophobic interactions”. This favorable interaction has been used to prepare CNF-based carbon inks for different applications, such as energy storage and sensing.[90–92]

2.5.3. Limitations of CNF-based conducting composites

Although CNFs provide excellent colloidal stability, mechanical strength, and stability to otherwise brittle conductive materials, there are limitations to the wide-scale applicability of these composite materials. A few of which are:

(1) The preparation of CNFs is an energy and time intensive process, commonly requiring microfluidization (atleast for most protocols). This thesis demonstrate the use of modified cellulose fibers for preparation of conductive composites.

(2) Since most of the conducting materials (carbon or conducting polymers) have a negative surface potential, the weak interactions between negatively charged CNFs and conducting materials create issues with the retention of these materials in the final composite, especially if traditional paper-making techniques are used. The use of cationic cellulose fibers helped address this challenge, as demonstrated in this work.

(3) Conducting materials, especially conducting polymers, are highly conductive but stiff and brittle. On the other hand, CNFs are non-conductive but provide excellent mechanical properties. Hence, there is a trade-off between desired conductivity and mechanical flexibility when changing the ratio of composite components. Therefore, it is essential to understand and tailor the interactions between these materials to obtain flexible, robust, and conductive composites. Different tools and methods were used to study these interactions and the knowledge created was used to tailor the properties of composites.

3. Materials and Methods

Below is the summary of materials, methods and characterization techniques used in this thesis. The methods are described in detail in the papers appended at the end of this thesis.

3.1. Materials

PEDOT:PSS (Clevios PH1000, Heraeus), CM-CNF (600 μeq/g, RISE Bioeconomy, Sweden), sulfite dissolving pulp (Aditya Birls Domsjö Fabriker AB, Sweden). Glycerol, sodium periodate, sodium borohydride, calcium chloride, sodium chlorite, sodium hypochlorite (14 vol%), dimethyl sulfoxide (DMSO), N-methylmorpholine N-oxide (NMMO), sodium chloride, TEMPO, GTMAC, and other reagents were purchased from Sigma Aldrich and used without further purification. Polyvinyl amine (PVAm) was purchased from BASF Gmbh, Germany. Silica coated QCM-D crystals were purchased from Q-sense AB, Sweden. Activated carbon (Norit A Supra, Acros Organics), cationic polyacrylamide (C-PAM, Kemira Fennopol K4230 T), carbon-black (CB, Thermo Scientific Alfa Aesar 039724.A1).

3.2. Methods

3.2.1. Preparation of TEMPO-oxidized cellulose

The method developed by Saito et al.[13] for TEMPO-mediated oxidation was followed to prepare TEMPO-oxidized cellulose fibers. Briefly, sulfite dissolving pulp was purified in acetate buffer (0.1M, pH 4.6) containing sodium chlorite (0.3 wt%) at 60°C for 1h. Afterward, the purified fibers were suspended in a phosphate buffer (0.1 M, pH 6.8) at 60°C. Subsequently, sodium chlorite, TEMPO, and sodium chlorite were added, and the reaction continued for 140 min under continuous stirring. The fibers were washed afterward with deionized water, and the total charge of fibers was measured with conductometric titration (Titrino 702 SM) according to the method described by Katz et al.[93] The average charge density (averaged over three repeated measurements) of 518 μeq/g was obtained.

3.2.2. Preparation of cellulose model surfaces for adsorption studies

Cellulose model surfaces were prepared according to the method reported by Gunnars et al.[6] TEMPO-oxidized cellulose fibers (0.25 g) were dissolved in NMMO (12.5 g) at 115 °C until the cellulose was dissolved. Next, DMSO (37.5 g) was dropwise added to the solution, and the temperature was increased to 125 °C. The dissolved cellulose solution was spin-coated on PVAm-adsorbed QCM crystals and regenerated by dipping the crystals in Milli-Q water for an hour. The crystals were dried with nitrogen, heated in the oven at 100 °C for 6h, and stored at room temperature before adsorption measurements.

For adsorption studies with CM-CNF, the QCM crystals were cleaned and inserted in the QCM-D instrument. First, the baseline (with Milli-Q water) was measured for 2h. Subsequently, PVAm (0.1 g/L, pH 7.5), CM-CNF (0.05 g/L, pH 6), and PEDOT:PSS (0.5 g/L, pH 3.5) adsorption was performed with washing (Milli-Q water) in between. The solutions were adjusted to the same pH and ionic strength as the adsorption experiments performed.

3.2.3. Preparation of Dialcohol-modified cellulose (DALC)

DALC fibers were prepared according to the method developed by Larsson et al.[28] Beaten bleached softwood kraft fibers (fines removed) were suspended in Milli-Q water at a concentration of 15 g/L and oxidized to dialdehyde cellulose using sodium periodate (1.35 g/g of fiber); under dark conditions and at the room temperature. The reaction time was varied to achieve a different degree of modification (DM); 12h, 24h, and 31h for DM 15, DM 30, and DM 44, respectively. After the reaction, the fibers were washed thoroughly with Milli-Q water. The carbonyl content was determined using an earlier described method, where protons released from the reaction of hydroxylamine with aldehyde groups were titrated.[29] The subsequent reduction of dialdehyde to dialcohol groups was performed by re-dispersing modified fibers in 0.01M phosphate buffer and performing the reduction reaction with sodium borohydride (0.4 g/g of fibers) for 3h. The reaction was stopped by removing the fibers from the reaction mixture and washing with Milli-Q water until the conductivity of the filtrate was <5 μS/cm.

3.2.4. Preparation of DALC/PEDOT:PSS inks for 3D-printing

Conducting inks were prepared by mixing DALC fibers and PEDOT:PSS in a ratio of 4:1, 3:2, and 3:7; glycerol (5 vol%) was added to the inks and stirred continuously for 1h. Inks were left in the fume hood to evaporate water and increase the solids content for 3D printing. The inks were printed using an Inkredible bioprinter (Cellink, Sweden).

3.2.5. Cationic modification of cellulose and PEDOT:PSS adsorption

Cationic cellulose fibers were prepared from sulfite dissolving pulp using the following procedure. First, dissolving pulp fibers (400 g) were mixed with 4.78M NaOH and left for 10 min. Afterward, the isopropanol (612 g) and GTMAC (400 g) were added to the slurry, and the reaction was carried out at 65 °C for 6h in a hot water bath. To stop the reaction, the mixture was neutralized with 1M hydrochloric acid, filtered, and washed thoroughly with Milli-Q water. The charge density of the pulp, 250 ± 50 μeq/g, was measured with polyelectrolyte titration. In total, 2 Kg of fibers were prepared for four paper machine trials.

To prepare PEDOT:PSS saturated cationic fibers, a fiber dispersion (2 g/L) was mixed with PEDOT:PSS (10 g/L, Orgacon ICP 1050, Agfa) and stirred for 30 min. The fibers were then filtered and washed to remove excess PEDOT:PSS.

3.2.6. Fabrication of conductive paper on the paper machine

The pilot production of paper was carried out on a 20 cm wide paper machine at Ahlström-Munksjö R&D center in Apprieu, France. Four different formulations, i) activated carbon, cationic pulp with PEDOT:PSS; ii) activated carbon, cationic pulp with PEDOT:PSS, CM-CNF; iii) activated carbon, cationic pulp with PEDOT:PSS, carbon black (CB) dispersed with CNF (10:1); iv) activated carbon, cationic pulp with PEDOT:PSS, CB dispersed with CM-CNF (10:1), CM-CNF; resulted into four different 10-meter paper rolls. The web speed was set to 1m/min, and the final drying of paper was performed in two steps- first drying between 138-180 °C and the second drying between 124-155 °C. The paper with a moisture content of 6% was collected into 10-meter webs winded on rolls.

3.3. Characterization Techniques

3.3.1. Charge determination

Conductometric titration: The total number of carboxyl groups on fibers were determined using conductometric titration (Metrohm 702SM Titrino titrator) according to SCAN-CM 65:02 standard.

Polyelectrolyte titration: The surface charge of the fibers was determined with a Stabino polyelectrolyte titrator. For negative surface charge determination, poly(diallyldimethylammonium chloride) (PDADMAC) polyelectrolyte was used; for positive surface charges, poly (vinyl sulfone) (KPVS) polyelectrolyte was used.

3.3.2. Quartz Crystal Microbalance with Dissipation (QCM-D)

QCM-D measurements were performed with QCM-E4 (Q-Sense AB, Sweden). All the experiments were performed at 25 °C (unless otherwise mentioned) at a flow rate of 0.15 ml/min.

The QCM-D crystals were coated with dissolved cellulose solution to prepare regenerated cellulose surfaces or used directly (in the case of in-situ adsorption of CM-CNF). The adsorption measurements were started after obtaining a stable baseline for at least 1 h. In the case of PEDOT:PSS adsorption on CM-CNF, the respective layers were adsorbed: firstly, the PVAm anchor layer was introduced; secondly, CM-CNF was introduced; thirdly, PEDOT:PSS was introduced into the QCM chamber. A washing step was performed after each layer. In regenerated cellulose films, the baseline was obtained, and PEDOT:PSS was introduced immediately after. The baseline was performed at the same temperature, pH, and ionic strength as that used in the adsorption measurements.

3.3.3. Structural Characterization

***Dynamic Light Scattering (DLS)*:** The particle size was measured using Zetasizer ZEN3600 (Malvern Instruments Ltd. UK) using disposable folded capillary cells. Zeta potential was measured using the same instrument by measuring the electrophoretic mobility of the particles.

***Scanning Electron Microscopy (SEM)*:** The surface and cross-section morphology and elemental analysis of the samples were analyzed using a Hitachi

S-4800 field-emission scanning electron microscope (FE-SEM) equipped with an energy dispersive x-ray detector (EDS). Before imaging, samples were coated with Pt/Pd unless otherwise mentioned. The cross-section samples in Article III were prepared by the solvent exchange to ethanol and critical point drying.

A focussed ion-beam SEM (FIB-SEM, Tescan GAIA3) equipped with an EDS detector was used to prepare and image the cross-section of individual DALC-modified fibers.

***X-ray scattering*:** An Anton Paar SAXSpoint 2.0 system with Microsource X-ray source (Cu Kα radiation with a wavelength of 0.15418 nm) and a Dectris 2D CMOS Eiger R 1M detector was used for wide angle x-ray spectroscopy (WAXS). The measurements were performed under vacuum; for each sample, three frames (each of 20 min) were read from the detector.

***Atomic Force Microscopy (AFM)*:** The samples were imaged using Multimode 8 (Bruker, USA). All the imaging was done under ambient conditions using SCANASYST-AIR cantilevers (Bruker, USA) in scanasyst mode. The QCM-D crystals were imaged directly after adsorption.

Colloidal probe AFM (CP-AFM) force measurements were performed using a MultiMode III (Veeco Instruments, USA) with picoforce extension. Tipless cantilevers (CSC37/NoAl Mikro-Masch, Germany) were mounted with spherical silicon dioxide probes (Duke Scientific, USA) and calibrated. In the case of CM-CNF and PEDOT:PSS interactions, probes were coated with two bilayers of poly(allyl hydrochloride) (PAH) and CM-CNF via dip coating and thorough rinsing in between the layers. PEDOT:PSS surfaces were prepared on PAH-coated silica wafers within an AFM liquid cell. The force curves were measured at different pH by injecting the solutions at that pH and allowing the surfaces to equilibrate for 30 min. Three measurements at five different locations were performed. The force curves were evaluated and averaged using AFM ForceIT software.

For DALC and PEDOT:PSS interaction, the colloidal probe was coated with a bilayer of PAH and PEDOT:PSS. The fibers were adsorbed on PAH-coated silica wafers, and the measurements were performed under similar conditions as mentioned previously.

3.3.4. Rheology

To measure the flow properties of inks, rheology measurements were performed using a DHR-2 rheometer (TA instruments, USA) with 25mm parallel-plate geometry at 25 °C. The samples were equilibrated for 10 min before analysis. The flow analysis was performed at a shear rate between 0.01 and 500 s^{-1}, and the measurements were performed in triplets.

3.3.5. Mechanical Testing

The rectangles of dimensions 50 mm * 5mm were tested under tension mode using an Instron 5944 Tensile Tester equipped with a 500N load cell. The samples were strained at a strain rate of 0.5 mm/min, until fracture. Before testing, the samples were conditioned at 23 °C and 50% relative humidity (RH).

3.3.6. Electrical and electrochemical characterization

***Electrical conductivity*:** The conductivity was measured using Keithley 2410 source meter and a two-probe configuration. The samples were used as rectangles (20 mm* 5mm). The resistance was calculated from the slope of I-V curve. Conductivity was measured using the formula: $\rho = L/(R*w*t)$; where ρ is the conductivity, L is the distance between the electrodes, w is the width, and t is the thickness of the sample.

CV and GCD: Electrochemical measurements were performed using BioLogic VSP potentiostat. Three-electrode setup was used for CV measurements, where Ag/AgCl (BASi, 3M NaCl) was the reference electrode, platinum was the counter electrode, and a 3D-printed sample mounted on a platinum wire was used as a working electrode. The electrodes were dipped in an aqueous electrolyte (1M H_2SO_4) for CV measurements.

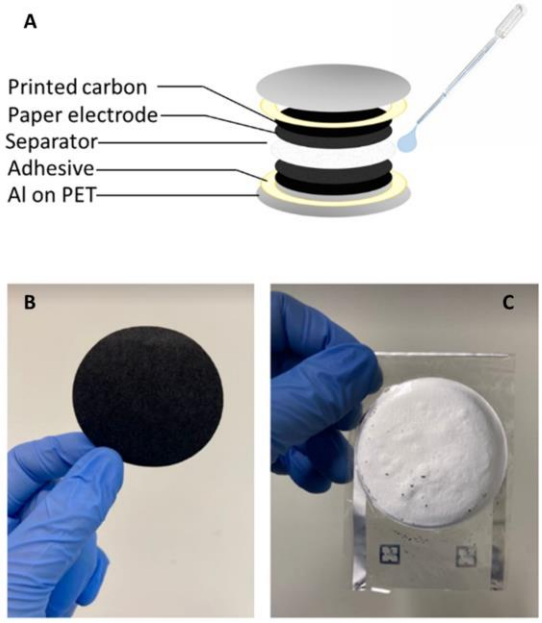

Figure 4 (A) Schematic of different parts of an assembled supercapacitor, (B) picture of the paper electrode, and (C) the assembled EDLC supercapacitor.

***Supercapacitor assembly*:** The supercapacitors were assembled from circular paper electrodes (5.5 cm) produced in a pilot paper machine, as shown in Figure 4. The circular separators (6.0, cleanroom wipes) and patches were prepared with a laser cutter; the final devices were mounted on carbon-printed collectors using carbon ink as glue. The separators were soaked in the ionic electrolyte and mounted on the electrodes. Finally, the device was assembled, laminated, sealed, and measured with CV.

4. Results and Discussion

This chapter of the thesis is divided into three sections. Firstly, the morphology of PEDOT:PSS complexes in solution is discussed based on both experimental analysis and computational modeling. Following this, the molecular interactions between cellulose and PEDOT:PSS and the factors that affect these interactions are discussed. The third and final section describes different chemical modifications that can be used to tailor the interactions between cellulose and PEDOT:PSS. In addition, the fabrication methods used to prepare cellulose and PEDOT:PSS composites are discussed, specifically how organic electronic devices can be prepared based on these composites.
These highlighted results are naturally only a summary of the research results and a more detailed description can be found in the appended papers.

4.1. PEDOT:PSS complexes in solution (Paper I)

PEDOT:PSS is a polyelectrolyte complex dispersed in water, as described previously. Since most computational and experimental research focuses on PEDOT:PSS films, particle behavior in solution has remained largely unexplored. Using both experimental methods and molecular dynamics (MD) simulations, the particle size, zeta potential, charge density, and the effect of solution parameters, such as pH and ionic strength, on PEDOT:PSS morphology were studied. For this purpose, the PEDOT:PSS was filtered with a syringe filter to remove larger aggregates.

4.1.1. Effect of pH and ionic strength on PEDOT:PSS

The particle size and zeta potential of PEDOT:PSS particles were determined using dynamic light scattering (DLS) and electrophoretic mobility using the same instrument. The charge density of the particles was also measured by polyelectrolyte titration using cationic poly(diallyldimethylammonium chloride) (PDADMAC). The diluted PEDOT:PSS dispersion at the concentration of 0.5 g/L had a pH of 3.5.

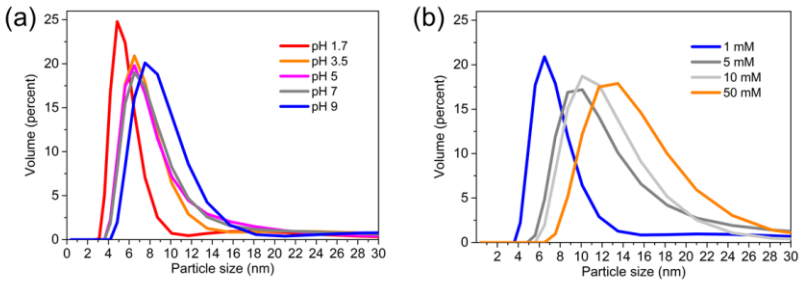

Figure 5 The particle diameter of PEDOT:PSS complexes measured via DLS at different (a) pH and (b) ionic strengths (pH was kept constant at 3.5). Adapted from Paper I.[94]

***Particle size*:** The particle size distribution at pH 3.5 (Figure 5a) showed that most PEDOT:PSS particles were less than 20 nm in diameter. A small fraction of particles measured 30 nm in diameter or greater, with some larger aggregates present, however their concentration was low compared to the majority of the particles. Similar particle sizes (16-20 nm) have been reported in earlier studies, using a variety of spectroscopic techniques.[95–97] Reducing the pH from 3.5 to 1.7 resulted in a decreased particle size from 16 to 12 nm, respectively, due to the partial protonation of PSS at the lower pH. Increasing the pH from 3.5 to 7 did not significantly affect the particle size, however at pH 9, the particle size increased to 19 nm. Similarly, an increase in ionic strength from 1mM to 50 mM showed an increase in particle size from 16 nm to 38 nm (Figure 5b).

The trends in particle size were possibly due to the change in PSS chain morphology within the polyelectrolyte complex. Specifically, at pH 1.7, the PSS is partially protonated, decreasing the ionic interaction between $PEDOT^+$ and PSS^-. Additionally, the $PEDOT^+$ counterions might be exchanged from PSS^- to Cl^-, leading to a smaller particle size. It should be additionally noted that lowering the pH also increases the solution's ionic strength, and thus reduces both intra- and inter-particle interaction among PEDOT:PSS complexes. As a result, the particles have the potential to form larger aggregates. This is evident in Figure 5 where at pH 1.7 the number of particles with a diameter of 30 nm slightly increases.

While a similar mechanism can explain the change in particle size with increasing ionic strength (and at pH 9), increasing the ionic strength will also lead to

decreased expansion of PSS chains on the surface of the PEDOT:PSS complexes, thereby reducing the particle size. Moreover, high pH and increased Na^+ concentrations lowers the charge of PEDOT and induces de-doping,[98,99] which can reduce the interaction between PEDOT and PSS and can cause destabilization in the system via association and aggregation of complexes. Overall the size of the PEDOT:PSS complexes is determined by the balance between inter- (macroscopic association between complexes) and intra-particle (PEDOT and PSS interaction, PSS chain expansion) interaction. Despite the variety of factors that impact the particle size of PEDOT:PSS complexes, no macroscopic aggregation was observed over a rather wide range of pH and ionic strengths, indicating good colloidal stability of the PEDOT:PSS complexes.

***Zeta potential and Charge density*:** The zeta potential of PEDOT:PSS complexes under various pH and ionic strengths is shown in Figure 6a and 6b, respectively. As expected, the zeta potential decreases while increasing both the pH from 3.5 to 9 and the ionic strength from 1 mM to 10 mM. Lowering the pH to 1.7 additionally showed a decrease in zeta potential. As discussed previously, the PSS chain extension as well as the charge balance between PEDOT and PSS both affect the zeta potential. In contrast to 5 and 10 mM, a slight increase in zeta potential was observed at 50 mM. While the cause for this increase is unclear, it is possible that the overall interaction between the PSS and PEDOT chains decreases due to the higher ion concentration moving inside the complexes. This may lead to a change in the overall structure and thus the stoichiometry of the complexes, but more investigations are needed to explain this behaviour more thoroughly.

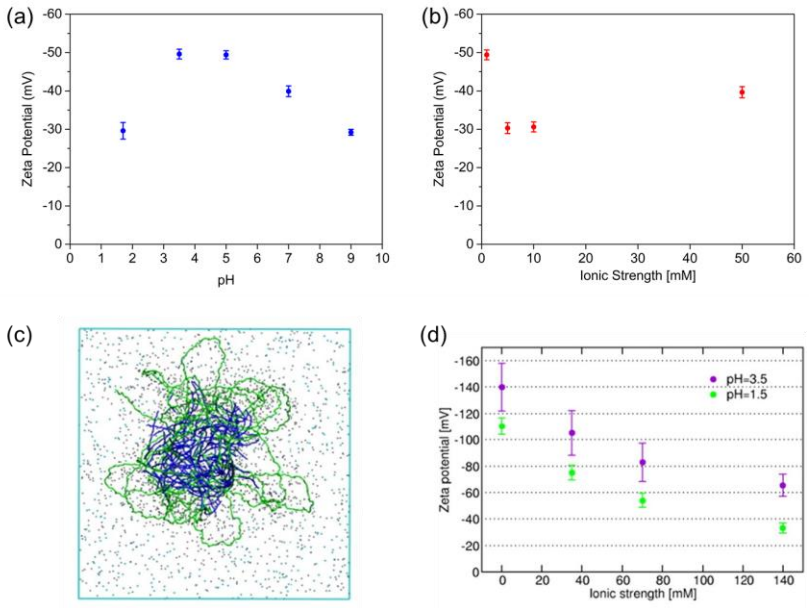

Figure 6 Zeta potential of PEDOT:PSS complexes measured at different (a) pH and (b) ionic strengths. (c) An image showing the morphology of the simulated PEDOT:PSS complex (blue color represents PEDOT and green color represents PSS chains) and (d) the simulated zeta potential values of PEDOT:PSS complex at different ionic strengths and pH. Adapted from Paper I.[94]

4.1.2. Computational microscopy of PEDOT:PSS

The particle size and zeta potential of PEDOT:PSS complexes in water were simulated using MD simulations and compared with the experimental data. The simulation details can be found in the appended paper (Paper I). Briefly, a PEDOT:PSS complex was modeled as a PEDOT core surrounded by the PSS shell, where the PSS chains were also found to penetrate the PEDOT core (Figure 6c). In addition to the PSS distribution, different ions, such as Na^+ and Cl^-, were also simulated at pH 1.5 and 3.5. The zeta potential at different pH and ionic strength was calculated based on simulated particle morphology. The particle diameter was estimated to be 25 nm at pH 3.5 and 18 nm at pH 1.5. At pH 1.5, PSS chains exhibited less expansions from the surface of the polyelectrolyte complex, and the

ion distribution showed a lower concentration of Na^+ inside the PEDOT:PSS, due to the partial protonation of PSS chains. As a result, a more compact structure was observed at pH 1.5 compared to pH 3.5. The zeta potential also decreased with increasing pH and ionic strength (Figure 6d). Qualitatively both the particle size and zeta potential from experimental and computational results show good agreement. As a result, MD simulations provide useful insight into the structure and the ion distribution of PEDOT:PSS complexes which otherwise would be difficult, if not impossible, to observe experimentally.

4.2. Interaction between PEDOT:PSS and cellulose (Paper II)

Materials made solely from PEDOT:PSS are conductive but brittle. In this respect, cellulose fibers and nanofibrils can provide a 3D network for preparing PEDOT:PSS composites with complex geometries and good mechanical properties. An essential aspect of cellulose/PEDOT:PSS composites is understanding the molecular interactions between the two components in dispersion or the wet state. Developing a thorough understanding of these interactions is crucial for the bottom-up design of conducting and functional materials. Hence, this section is dedicated to understanding the fundamental aspects of the interaction between PEDOT:PSS and cellulose.

4.2.1. Adsorption of PEDOT:PSS onto cellulose and factors affecting the interactions

The adsorption of PEDOT:PSS onto cellulose was investigated using quartz crystal microbalance with dissipation (QCM-D). QCM-D monitors the sensor's resonance frequency change upon the adsorption of material, including solvent molecules associated with that material. This change in frequency can be translated to the adsorbed mass using the Sauerbrey equation[100]:

$$m = C(\Delta f/n) \qquad \text{(Eq. 3)}$$

where m is the adsorbed mass, C is the Sauerbrey coefficient, Δf is the frequency change, and n is the overtone. The energy dissipation, related to the rigidity of the adsorbed layer, can also be evaluated via dissipation measurements.

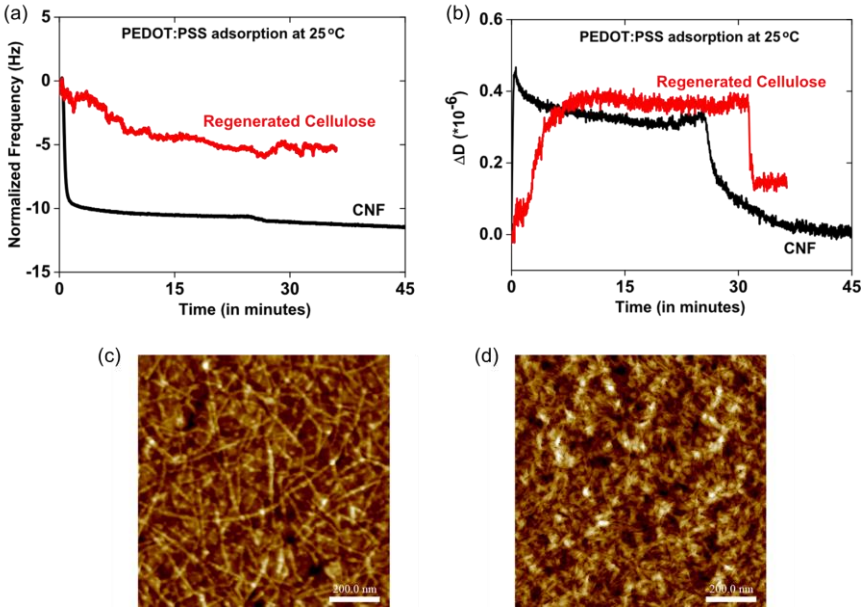

Figure 7 QCM-D measurements of PEDOT:PSS adsorption on CM-CNF and, TEMPO-oxidized regenerated cellulose surface at pH 3.5 showing (a) frequency and (b) dissipation. AFM images of the QCM model surfaces after PEDOT:PSS adsorption on (c) CM-CNF and (d) regenerated cellulose. Adapted from Paper II.[101]

QCM-D results from adsorption measurements of PEDOT:PSS on regenerated cellulose films (TEMPO-oxidized fibers dissolved in NMMO/DMSO and regenerated in water) and CM-CNF are shown in Figure 7a. PEDOT:PSS was found to adsorb to both regenerated cellulose and CM-CNF, as indicated by the decrease in frequency upon injection of PEDOT:PSS. This adsorption demonstrates an attractive interaction between the anionically charged PEDOT:PSS and the anionic cellulose surfaces. The kinetics of adsorption differed for the two substrates, with spontaneous and rapid adsorption occurring for CM-CNF, and a slower adsorption process occurring at the regenerated cellulose surface. Moreover, the adsorbed layers were found to be rigid for both CM-CNF and regenerated cellulose, as indicated by the relatively small and rapid change in dissipation (Figure 7b). AFM images of the films following adsorption showed that the PEDOT:PSS particles had

a pearl-necklace-like morphology on the CM-CNF surface (Figure 7c), whereas no such structures could be observed on regenerated cellulose surfaces (Figure 7d). Table 1 presents how different solution parameters, such as temperature, pH, ionic strength, and CM-CNF counterion, affect the adsorption of PEDOT:PSS onto CM-CNF surfaces. For all the solution parameters, detailed QCM curves can be found in Paper II. The factors responsible for these changes and their effects on adsorption can be understood as follows:

Table 1: Factors affecting the adsorption and the corresponding amount of PEDOT:PSS adsorbed onto CM-CNF (the total mass also includes the amount of water adsorbed). Adapted from Paper II.[101]

Factors affecting the adsorption	Total adsorbed mass of PEDOT:PSS per mg of CNF (mg/mg)
Temperature (°C)	
25	0.16
40	0.58
pH	
3.5	0.16
5	0.07
7	0.01
Ionic strength (mM)	
0	0.16
10	0.52
50	0.68
Type of counterions	
Na^+	0.16
Ca^{2+}	0.24
Fe^{3+}	0.18

i) *Temperature*: Increased adsorption with increasing temperature indicates that the adsorption of PEDOT:PSS onto CM-CNF is an entropy-driven process.[102] This process can be understood as a balance between the entropy loss of PEDOT:PSS following adsorption and the entropy gain from the release of structured water from the cellulose surface (Figure 8a). The QCM results demonstrate that the entropic gain due to the release of water is dominant, and thus PEDOT:PSS adsorbs to the cellulose surface.

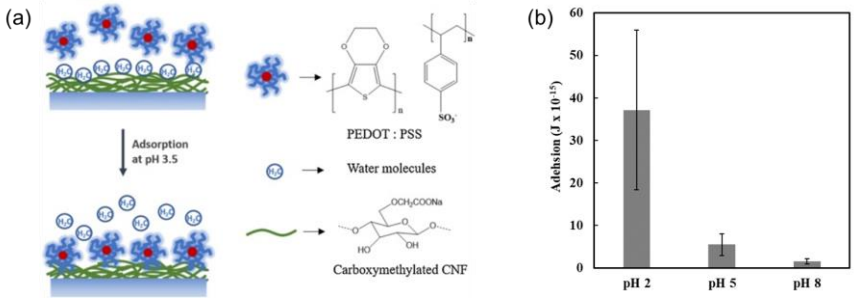

Figure 8 (a) A schematic image showing the release of water molecules upon adsorption of PEDOT:PSS on cellulose; (b) Adhesion between CM-CNF coated colloidal probe and the PEDOT:PSS surfaces as calculated as an integral of the force-displacement curves from the AFM colloidal probe measurements. Adapted from Paper II.[101]

ii) *pH*: Table 1 shows that significantly more PEDOT:PSS adsorbs to CM-CNF surfaces at lower pH. The pK_a of carboxyl groups is ~4, and thus a significant amount of the CM-CNF surface charge groups are deprotonated, resulting in a negatively charged surface at pH > 4.[103] At pH 3.5, protonation of carboxyl groups lowers the repulsive interactions between the negatively charged PEDOT:PSS and the CM-CNFs and therefore, more adsorption occurs. Similar results have been shown in the case of PEDOT:PSS adsorption onto microcrystalline cellulose (MCC).[77,78] Additionally, colloidal probe-atomic force microscopy (CP-AFM) measurements show a higher adhesion between a CM-CNF coated colloidal probe and a PEDOT:PSS substrate as the pH decreases from pH 8 to pH 2, further supporting the adsorption data from the QCM-D measurements (Figure 8b).

iii) *Ionic strength*: Increasing the ionic strength (at pH 3.5 and 25 ºC) from 0 mM NaCl to 50 mM NaCl increased PEDOT:PSS adsorption (Table 1). This is potentially due to screened charges between CNF and PEDOT:PSS, as well between the adsorbed PEDOT:PSS complexes on the surface. Screening decreases the repulsive interactions which work against the entropic driving forces of adsorption. AFM images of the QCM surfaces following adsorption at high ionic strength additionally show that PEDOT:PSS adsorbed as larger aggregates as compared to the low ionic strengths (Figure 9a, 9b). While Paper I demonstrated that the particle size of PEDOT:PSS did not change significantly in dispersion upon increasing the ionic strength the larger aggregates observed via AFM are suggested to be due to a surface induced association of PEDOT:PSS complexes at the CNF surface and potentially the formation more aggregated structures following drying.

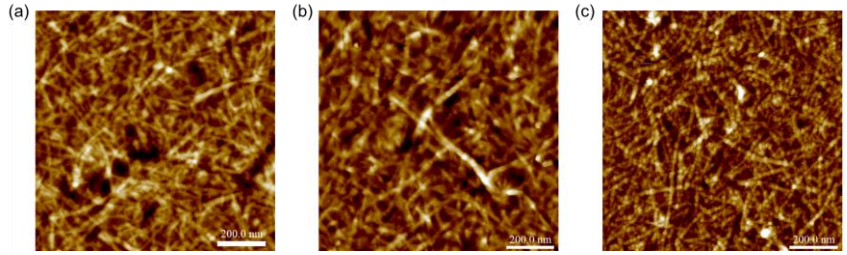

Figure 9 AFM images showing PEDOT:PSS particles adsorbed on CM-CNF at an ionic strength corresponding to (a) 10mM NaCl, (b) 50mM NaCl, and (c) the adsorption in the presence of Ca^{2+} (instead of Na^{+}) as a counterion. Adapted from Paper II.[101]

iv) *Counterions*: Exchanging the monovalent Na^{+} to divalent Ca^{2+} increased PEDOT:PSS adsorption to CM-CNF surfaces (Table 1, Figure 9c). The higher entropic gain from the release of counterions in presence of multivalent ions potentially can explain the increased PEDOT:PSS adsorption. Moreover, multivalent ions can act as a bridge between the two surfaces, inducing an attractive interaction.[104,105] Counterintuitively, a further increase in valency in the form of Fe^{3+} did not significantly increase adsorption compared to Na^{+}. While the specific mechanism is unclear the behaviour potentially could be due to the chelating properties iron, which can induce cross-linking within the CNF network,[106]

resulting in a reduced surface area and stronger self-association of CNFs that limits PEDOT:PSS adsorption.

To summarize, low pH, high ionic strength, and multivalent ions can increase the adsorption of PEDOT:PSS onto anionic CM-CNF surfaces. Moreover, the release of water molecules from the CNF surface is the dominant interaction which leads to adsorption of anionic PEDOT:PSS to anionic CM-CNF.

4.3. Cellulose modification for fiber-based conductive composites (Paper III, IV, V)

Despite the interaction between CNF and PEDOT:PSS, cellulose is an insulating material and thus hampers the conductivity of PEDOT:PSS. As a result, large amounts of PEDOT:PSS are required in cellulose composites to achieve desired properties. Additionally, when paper-making techniques are used to produce conductive composites, retention of PEDOT:PSS and CNF is a significant challenge. Therefore, chemical modification of cellulose is a potential route to tailor interactions and address the challenges of making conductive composites more scalable and efficient. This section describes two such chemical modifications for the preparation of conductive cellulose composites. Specifically, (i) dialcohol-modified cellulose (DALC) fibers and (ii) cationic cellulose fibers. In addition, two scale-up strategies, 3D printing and pilot paper machine production, are discussed for the production of biopotential monitoring electrodes and energy storage papers, respectively.

4.3.1. Dialcohol-modified cellulose (DALC) fiber-based conductive composites (Paper III, IV)

PEDOT:PSS is a high-performing, but expensive material. Therefore, it is natural to strive for good performance while reducing the amount of conductive material. Previous research has utilized nanocellulose to make mechanically-robust and printable conductive composites, however, nanocellulose is itself an energy and cost-intensive material. In comparison DALC fibers can be produced in an energy efficient way and have structures that resemble polyols like glycerol, sorbitol, etc., that are used to increase the conductivity of PEDOT:PSS. Moreover the open-chain structure high density of hydroxyl result in fibres which have been shown to be

considerably more flexible and ductile than to non-modified fibers.[28] Thus DALC fibers are an attractive material from the production of conductive composites with PEDOT:PSS via printing.

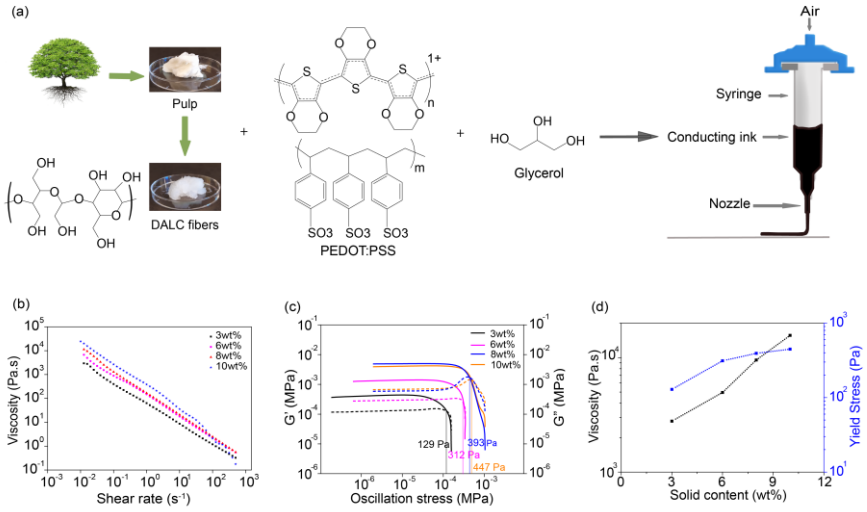

Figure 10 (a) Schematic summary of the components within the conducting ink and the 3D-printing process. Rheology analysis of 3D printable ink showing (b) viscosity as a function of shear rate, (c) storage modulus (solid lines) and loss modulus (dashed lines) as a function of oscillation stress, (d) viscosity (at a shear rate of 0.1 s^{-1}) and yield stress, as a function of a solids content of the conducting ink with DALC/PEDOT:PSS of 3:2 ratio. Adapted from Paper III.

3D-printable inks of DALC fibers and PEDOT:PSS

DALC fibers and PEDOT:PSS were mixed at different dry weight ratios, 4:1, 3:2, and 3:7, respectively, to form conductive inks. All inks were produced using DALC fibres with a degree of modification of 44% (percentage of modified glucan chains within the fiber) and the addition of 5 vol% glycerol. Samples were printed using an extrusion-based 3D-bioprinter (Figure 10a), dried in an oven at 60˚C, and characterized. The rheological characterization of inks at different solids content demonstrates that all inks have the proper shear thinning behavior that is required for printing (Figure 10b, 10c, 10d). Samples printed in different 3D shapes (Figure 11a), indicates the formation of a cross-linked network within and across each layer. The electrical conductivity of the 3D printed samples increased from 10 S/cm to 30 S/cm, when increasing the PEDOT:PSS content from 20 to 40% (4:1 to 3:2), from

which saturation occurs at 70% (3:7) PEDOT:PSS (Figure 11b). Samples demonstrated good conductivity in both water and PBS buffer, and remained conductive even after storing them for 90 days (Figure 11c).

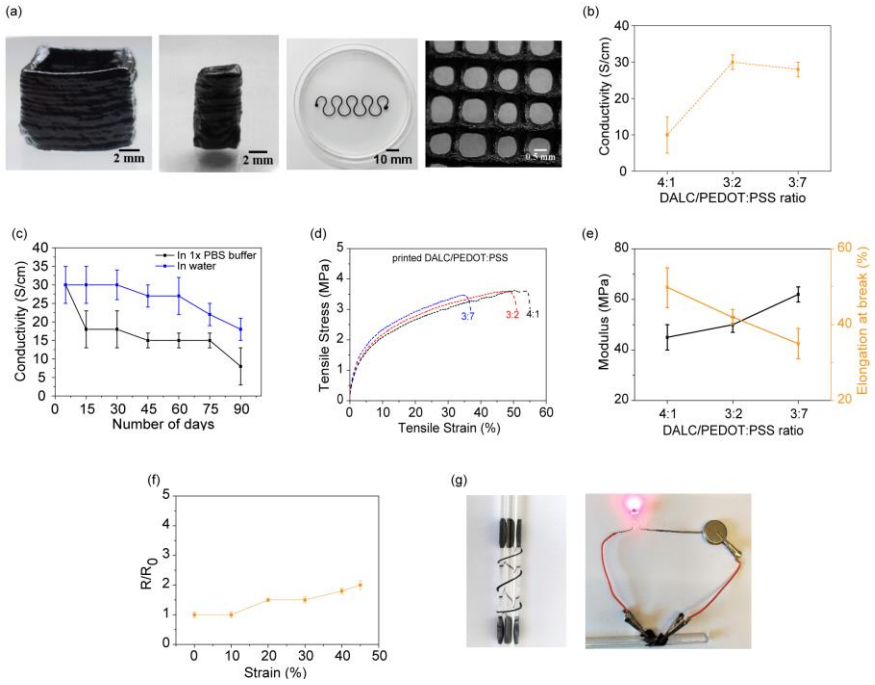

Figure 11 (a) Optical micrographs of 3D and 2D printed patterns in the shape of a 20-layered hollow cube, a hollow cylinder, a 5-layered serpentine pattern, and a 5-layered mesh structure, respectively. Electrical conductivity of (b) 3D-printed films as a function of DALC/PEDOT:PSS weight ratio, and (c) 3D-printed films soaked in water or PBS (1x) buffer as a function of the number of days of soaking. (d) Tensile stress-strain curves for dry composites, (e) Modulus and elongation at break, evaluated in tension, as a function DALC/PEDOT:PSS ratio, (f) Relative resistance change in a printed DALC/PEDOT:PSS (3:2) film under strain, evaluated in tension, (g) A printed serpentine pattern and film wrapped around a glass rod with a radius of 3 mm. Adapted from Paper III.

The mechanical characterization of the printed samples indicates that a strong and strainable network has been formed within the composite. A elastic modulus of 48 MPa and strain-at-break of 45% at a DALC/PEDOT:PSS ratio of 3:2 (Figure 11d, 11e) shows that DALC fibers act as a plasticizing agent for the PEDOT:PSS complex, similar to other hydroxyl groups containing compounds.[107] While DALC fibers allow for flexibility, they additionally provide stiffness when compared to

PEDOT:PSS/glycerol films, which were reported to have a modulus of 20 MPa.[107] Ouyang et al.[107,108] showed that compounds with hydroxyl groups could lower the interchain interaction between PSS chains and help increase the strainability of PEDOT:PSS films. Since DALC fibers have a flexible, ring-opened glucan chain structure and a high concentration of hydroxyls, a similar mechanism could occur within DALC/PEDOT:PSS composites. Furthermore, the low relative resistance change upon stretching (Figure 11f) and the maintained conductivity (glowing LED-light) after bending (Figure 11g) demonstrates that an excellent interface is formed between PEDOT:PSS and DALC fibers.

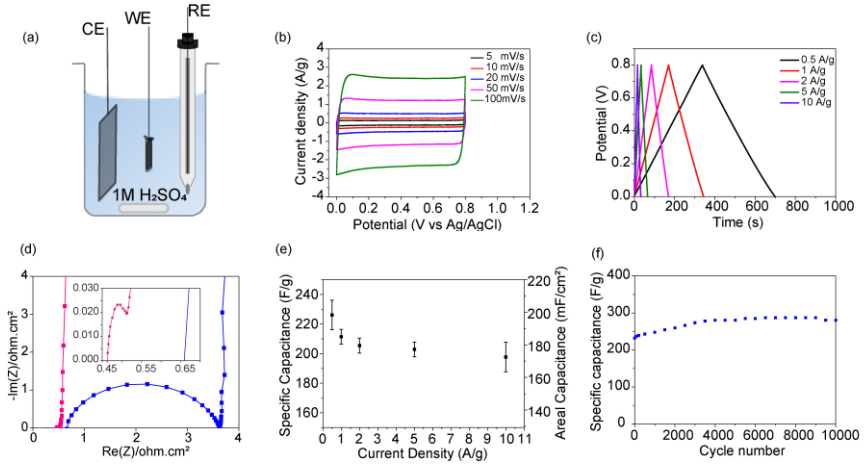

Figure 12 Electrochemical measurements: (a) schematic 3-electrode setup consisting of reference electrode (RE- Ag/AgCl), counter electrode (CE- Pt electrode) and working electrode (WE- 3D-printed sample mounted on Pt wire). (b) Cyclic voltammetry curves at different scan rates. (c) Galvanostatic charge-discharge curves at different current densities. (d) Electrochemical impedance spectroscopy spectra for 3D-printed samples, before (blue curve) and after (pink curve) 10 000 charge-discharge cycles. The inset shows the magnification of high frequency region of the impedance spectra. (e) Specific capacitance (F/g) and areal capacitance (mF/cm^2) as a function of current density. (f) Normalized specific capacitance as a function of the number of charge-discharge cycles. Adapted from Paper III.

In addition to the electrical properties, printed composites displayed excellent electrochemical performance, as characterized by a 3-electrode set-up (Figure 12a). The quasi-rectangular shaped CV curves (Figure 12b) and the linear charge-

discharge curves (Figure 12c) of the printed electrodes indicate an electric double layer capacitive behavior.[58] The printed electrodes exhibited a high specific capacitance of 211 F/g (normalized to PEDOT mass), and areal capacitance of 200 F/cm² at 1 A/g (at a PEDOT:PSS content of 40%) (Figure 12e), compared to the theoretical capacitance of 210F/g for PEDOT.[109] Furthermore, the improvement in capacitance after 10000 charge-discharge cycles and the disappearance of a semi-circle in EIS spectra (Figure 12d, 12f) demonstrate a low internal resistance in the composites before cycling. This resistance was even lower after cycling. Overall, DALC/PEDOT:PSS composites form a robust, flexible, and conductive network, despite having a relatively low PEDOT:PSS content.

Factors affecting composites' properties

The degree of modification (DM) of the DALC fibers and the addition of glycerol was found to significantly affect the properties of DALC/PEDOT:PSS composites (Figure 13a). Since the inks with a DALC/PEDOT:PSS ratio of 3:2 showed the highest conductivity, all the further analyses were performed at the same composition. DALC/PEDOT:PSS/glycerol samples prepared with different DMs showed an increase in conductivity with increasing DM (Figure 13a, blue curves). Increasing DM results in a higher concentration of primary alcohol groups, which have been shown to increase the conductivity and plasticization of PEDOT:PSS chains. [29,30,108]

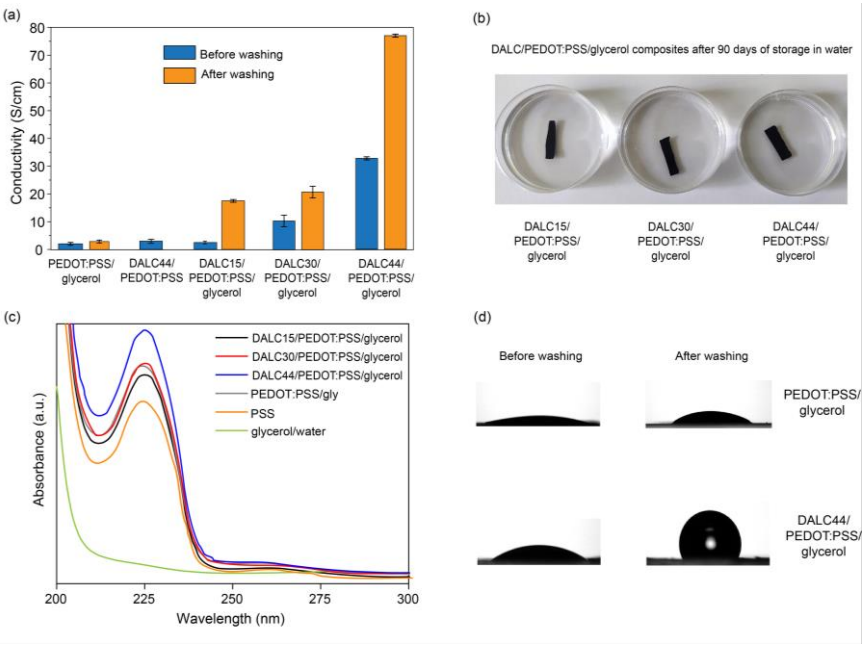

Figure 13 (a) Electrical conductivity before and after washing in water for PEDOT:PSS/glycerol, DALC/PEDOT:PSS, and DALC/PEDOT:PSS/glycerol composite films prepared with fibers modified to different degrees of modification; (b) Photographs demonstrating the wet stability of DALC/PEDOT:PSS/glycerol composites after 90 days of storage in water; (c) UV-visible spectra of the filtrate collected after washing the films; (d) Contact angle of water against PEDOT:PSS/glycerol and DALC44/PEDOT:PSS/glycerol films, before and after washing. Adapted from Paper IV.

The difference in conductivity of the DALC44/PEDOT:PSS samples with and without glycerol (Figure 13a) indicates that glycerol is essential not only for wet stability (Figure 13b), but also for good conductivity. Specifically, conductivity increased 10x from 3 S/cm for DALC44/PEDOT:PSS to 30 S/cm in DALC44/PEDOT:PSS/glycerol. In comparison, the addition of only glycerol to PEDOT:PSS did not result in a higher conductivity, indicating the combination of DALC fibers and glycerol was essential for good electrical performance (and durability in water).

Mechanism for conductivity enhancement

Conductivity enhancement in PEDOT:PSS has been attributed to the separation and removal of PSS, and the restructuring of PEDOT chains by secondary dopants.[52,54] A two-fold increase in conductivity after washing (Figure 13a, orange curves), a high intensity signal at 225 nm (for PSS) in UV-visible spectra (Figure 13c) of the washing solution, and a significant increase in contact angle in washed films (Figure 13d) strongly indicate the removal of PSS[110] and enrichment of the surface with hydrophobic PEDOT within DALC/PEDOT:PSS/glycerol composites upon washing with water.[111,112]

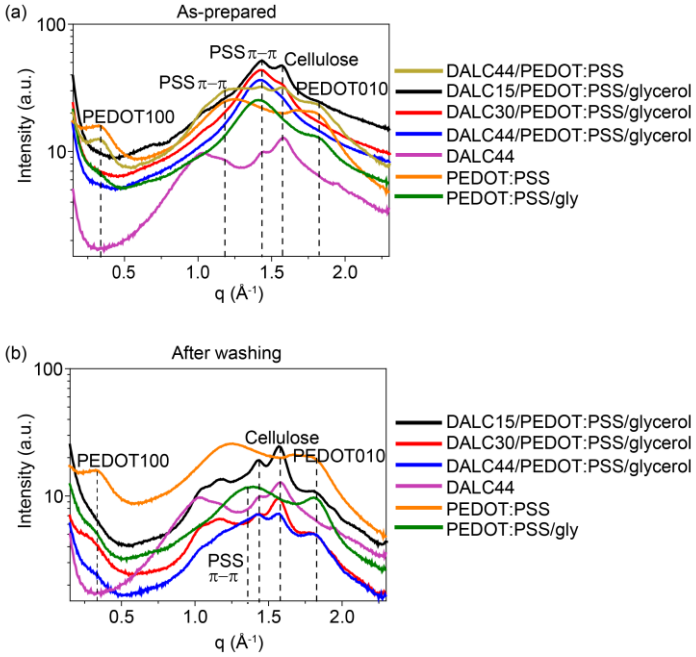

Figure 14 WAXS spectra of (a) as-prepared and (b) after washing for PEDOT:PSS, PEDOT:PSS/glycerol, DALC44/PEDOT:PSS, and DALC/PEDOT:PSS/glycerol films prepared with fibers modified to different degrees of dialcohol modification. Adapted from Paper IV.

WAXS spectra of the as-prepared and washed films (Figure 14a, 14b) suggests different PEDOT and PSS packing within the composite materials due to the addition of both the DALC fibers and glycerol. The critical peaks for PEDOT (0.3 Å-

$^{-1}$ and 1.8 Å^{-1}) and PSS (1.25 Å^{-1}) packing were masked by an intense peak at 1.4 Å^{-1} and 1.6 Å^{-1} in the DALC/PEDOT:PSS composites (Figure 14a). The peak at 1.4 Å^{-1} is presumably an overlapping peak between DALC fibers and a shifted peak of PSS (1.25 Å^{-1} to 1.4 Å^{-1}), indicating a close packing of PSS on DALC fibers. This shift also suggests a closer packing of PEDOT:PSS particles in DALC/PEDOT:PSS/glycerol composites. After washing, the intensity of the peak at 1.4 Å^{-1} reduced significantly (Figure 14b). Simultaneously, two peaks corresponding to PEDOT appeared, one at 0.3 Å^{-1} and another at 1.8 Å^{-1} (Figure 14b). However, DALC/PEDOT:PSS composites without any glycerol did not display such a peak shift, suggesting that glycerol is needed (in addition to DALC fibers) for better PEDOT and PSS packing. 3D printable inks with different DALC/PEDOT:PSS ratios also showed similar behavior before and after washing (see Paper III for more details).

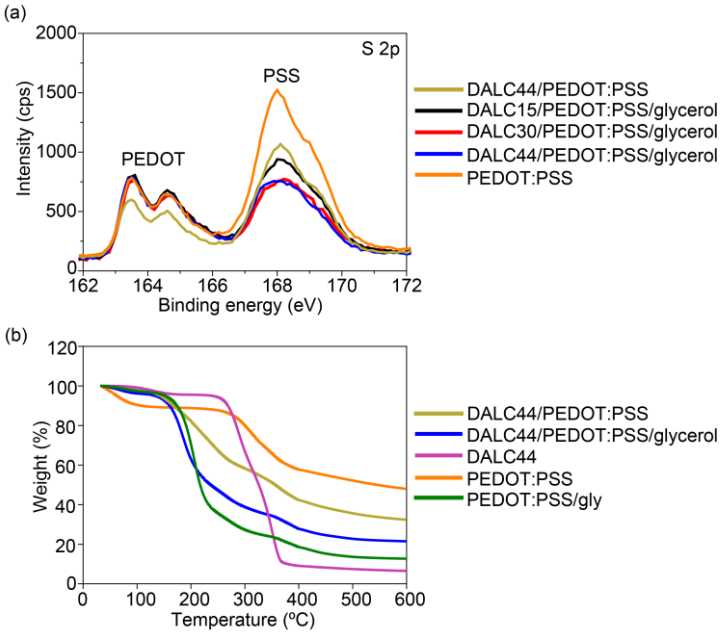

Figure 15 (a) XPS spectra, and (b) TGA curves, for PEDOT:PSS, PEDOT:PSS/glycerol, DALC44/PEDOT:PSS, and DALC/PEDOT:PSS/glycerol films prepared with fibers modified to different degrees of dialcohol modification. Adapted from Paper IV.

X-ray photoelectron spectroscopy (XPS) of washed DALC/PEDOT:PSS/glycerol composites (Figure 15a) indicate that the concentration of PSS (binding energies above 166 eV)[113] decreased with increasing DM of the DALC fibers. This suggests that the PEDOT concentration was increased (Figure 15a, binding energies below 166 eV)[113] and possibly reached the same as in the pure PEDOT:PSS films. Thus, further supporting that increased conductivity is due to PSS removal and PEDOT enrichment and organization, similar to other reported secondary dopants.[114]

The plasticizing effect of hydroxyl containing compounds on PSS interchain interaction has been shown to weaken the PEDOT and PSS interaction.[51,115] Thermal gravimetric analysis (TGA) of DALC/PEDOT:PSS and DALC/PEDOT:PSS/glycerol composites also showed this plasticizing effect (Figure 15b). DALC/PEDOT:PSS films exhibited similar thermal weight loss behavior as PEDOT:PSS/glycerol films. DALC/PEDOT:PSS/glycerol composites were less thermally stable. This indeed supports the suggested plasticization of PEDOT:PSS by DALC fibers and glycerol.[116,117]

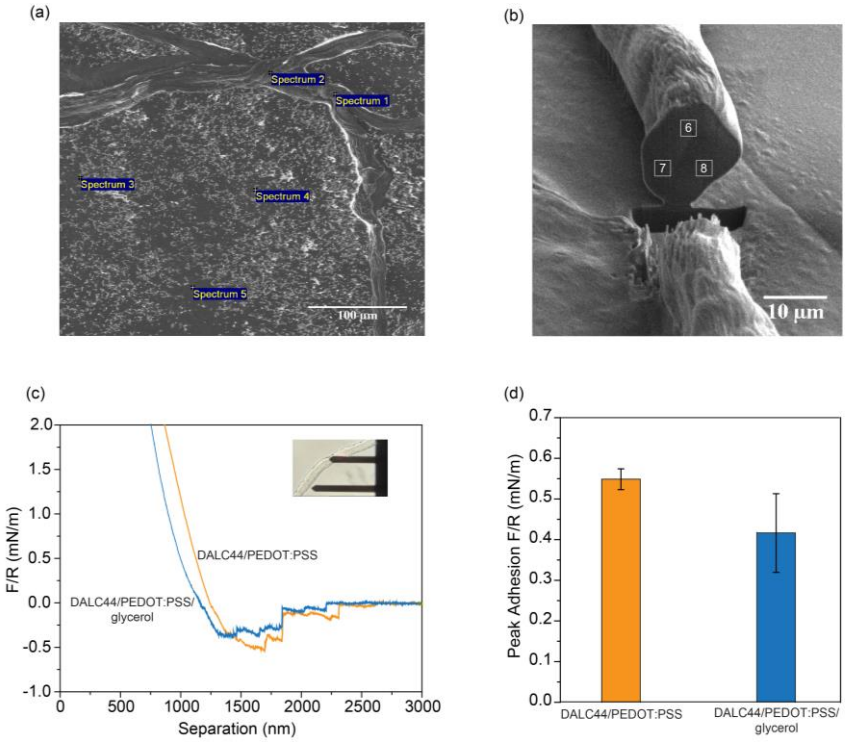

Figure 16 (a) SEM image showing the morphology of DALC44 fibers after the adsorption of PEDOT:PSS with marked points for the EDX spectra (data shown in Table 2); (b) a FIB-SEM image showing the freshly revealed cross-section of a single DALC44 fiber with adsorbed PEDOT:PSS (EDX intensities shown in Table 2); (c) radius-normalized colloidal probe force measurements as a function of separation (the inset shows the image of a DALC fiber without any PEDOT:PSS and the cantilever with PEDOT:PSS coated probe) and (d) peak adhesion, between a PEDOT:PSS-coated probe and a DALC44 fiber surface in pH 2 water, with and without glycerol**.** Adapted from Paper IV.

Interactions between DALC fibers, PEDOT:PSS and glycerol

DALC fibers act as a secondary dopant to PEDOT:PSS, but a deeper understanding of the molecular interaction is needed in order to control the structure and properties of these composites. PEDOT:PSS adsorbs spontaneously to DALC fibers (on the fiber surface as well as inside the fiber wall) when the two are mixed. Following PEDOT:PSS adsorption, DALC fibers were studied via scanning electron

microscopy (SEM) and energy dispersive x-ray spectroscopy (EDS). Both the surface of the fibers (Figure 16a) and the cross-section, revealed by focussed ion-beam SEM (FIB-SEM) (Figure 16b) were studied. Investigating the morphology, individual PEDOT:PSS complexes could not be distinguished despite the fibers having a blue appearance and being conductive. In fact following PEDOT:PSS adsorption the fibers were sufficiently conductive as they did not require Pt/Pd coating to prevent specimen charging during imaging. Chemical analysis via EDS showed the presence of sulfur both on the fiber surface and throughout the cross-section (Table 2), confirming PEDOT:PSS adsorption.

The interaction between PEDOT:PSS and DALC fibers was not significantly affected by the presence of glycerol. This evidenced by the fact that the adhesion between a PEDOT:PSS coated colloidal probe and DALC fibers remained relatively unchanged following the addition of glycerol to the cell. (Figure 16c, 16d). Since DALC fibers are highly hydrated[118] and have an abundance of primary alcohol groups, entropic interactions (similar to PEDOT:PSS adsorption on CM-CNFs) are a potential driving force for the adsorption of PEDOT:PSS. Moreover, dipole-dipole interactions between the polar surface of DALC fibers and PEDOT:PSS could play a role in the apparent irreversible nature of the adsorption.

Table 2: Elements detected by EDX at different locations in SEM image (Figure 16a, 16b). Adapted from Paper IV.

Location	Point spectra number	Sulfur (S) wt%	Carbon (C) wt%	Oxygen (O) wt%	Sodium (Na) wt%
On the fiber surface	Spectrum 1	8	72	17	3
	Spectrum 2	19	67	11	3
	Spectrum 3	0	89	11	0
	Spectrum 4	0	87	13	0
	Spectrum 5	0	85	15	0
In the fiber cross-section	Spectrum 6	47	32	4	17
	Spectrum 7	39	35	4	22
	Spectrum 8	37	38	5	20

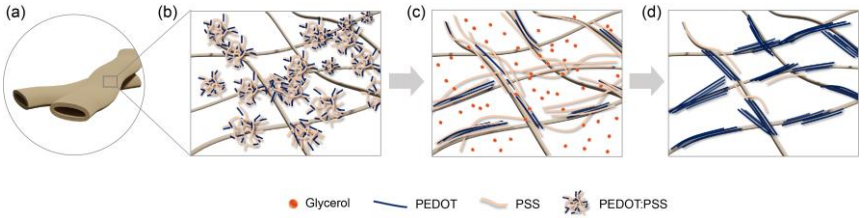

Figure 17 A schematic representation of the morphological model proposed to understand the effect of DALC fibers on the restructuring of the PEDOT:PSS showing (a) DALC fibers, (b) the random orientation of PEDOT:PSS particles adsorbed on DALC fibrils constituting the fiber-wall of DALC fibers, (c) segregation of PSS and stacking of PEDOT when glycerol was added to DALC/PEDOT:PSS inks, and (d) PEDOT enrichment on the surface after washing away excess PSS and glycerol from the DALC/PEDOT:PSS/glycerol composites. Adapted from Paper IV.

Based on the variety of characterization methodologies used, the interaction between DALC fibers, PEDOT:PSS, and glycerol can be summarized as follows. Upon mixing, PEDOT:PSS spontaneously adsorbs onto the nanofibrils that constitute the DALC fiber wall (Figure 17a). In the presence of glycerol, a portion of the PSS is removed and the PEDOT restructures into an extended conformation on the DALC fibers (Figure 17b). During drying a local increase in ionic strength and glycerol concentration further weakens the interactions between PEDOT and PSS leading to enrichment of PSS which can be washed away in water (Figure 17c). Simultaneously, the increased concentration of PEDOT makes the material more conductive and the surface more hydrophobic (Figure 17d). To conclude, DALC fibers induce a supramolecular structuring of PEDOT in DALC/PEDOT:PSS composites and glycerol strengthens interaction further by facilitating removal of PSS.

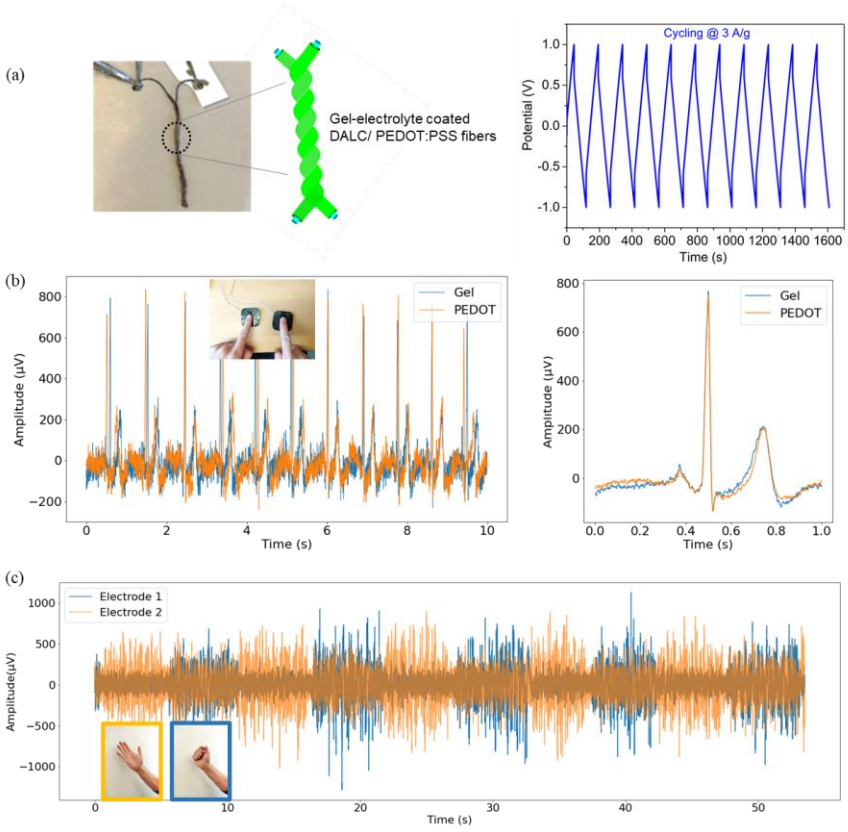

Figure 18 (a) A photograph and schematic drawing of a twisted supercapacitor consisting of 3D printed DALC/PEDOT:PSS fibers coated with gel electrolyte, and galvanostatic charge/discharge curves showing ten charge-discharge cycles, of the twisted supercapacitor device. (b) 3-lead ECG measurement signals (inset showing the measurement setup) detected using DALC/PEDOT:PSS electrode (orange) and a commercial gel electrode (blue). (c) EMG traces recorded while opening and closing a fist. Adapted from Paper III.

Applications of DALC/PEDOT:PSS composites

Printable, soft, stretchable and conductive biocomposites have numerous applications, particularly in bioelectronics.[53,119] The excellent flow properties of DALC/PEDOT:PSS inks aided in extruding long, conducting filaments. To synthesize a symmetric supercapacitor two of these filaments were soaked in a gel

electrolyte of polyvinyl alcohol and sulfuric acid (PVA/H_2SO_4) and twisted together after drying (Figure 18a). This device showed a high specific capacitance of 123 F/g at a current density of 3A/g, which could be used in wearable energy storage devices. Biopotential monitoring is yet another application for conducting polymer electrodes.[120] To demonstrate the potential of DALC/PEDOT:PSS composites in these applications printed electrodes were produced for biomonitoring. The printed electrodes showed very low impedance (few ohms), compared to other commercial electrodes (in kiloohms) in EC-12 tests (a standardized test used for disposable electrocardiography (ECG) electrodes). Furthermore, real-time ECG signals from the heartbeat and electromyography (EMG) signals (muscle potential) from opening and closing the fist were measured using the printed DALC/PEDOT:PSS/glycerol electrodes (Figure 18b, 18c). The versatility of DALC/PEDOT:PSS electrodes in combination with their high conductivity (even at low conducting polymer content) make them excellent candidates for bio-based electrodes in wearable and flexible electronics.

4.3.2. Conductive composites from cationic cellulose fibers (Paper V)

The challenges associated with the scalable production of anionic CNF-based conductive composites have been described in detail earlier (Section 2.5). However, by using cationic cellulose fibers, some of these challenges, such as retention of the active electrode materials in the nm-μm particle size range, can be overcome. Since the majority of the carbon materials and conductive polymers used for energy storage have a negative surface potential, cationic cellulose fibers can improve the adsorption and retention of these active materials during paper production via charge-mediated interactions. For this purpose, cationic fibers were prepared by grafting quaternary trimethyl ammonium groups onto the surface of cellulose fibers under highly alkaline conditions. The charge density used in this work was measured to be 300 μeq/g.

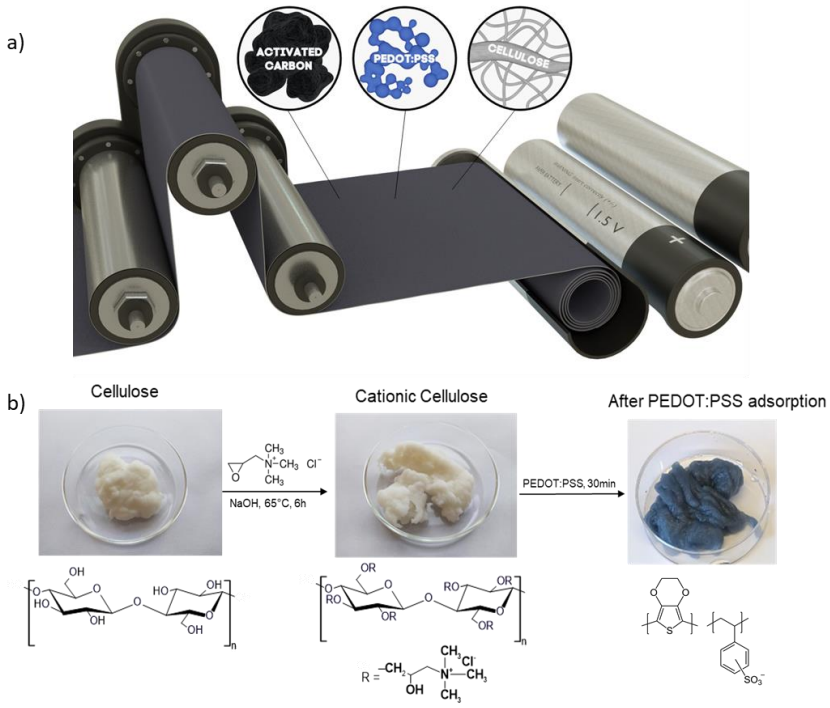

Figure 19 (a) A schematic description of the material concept and the papermaking process, and (b) The chemistry used for the paper machine trials with the cationization of pulp fibers with glycidyl trimethylammonium chloride and subsequent PEDOT:PSS adsorption. Adapted from Paper V.[121]

An earlier reported study showed good performance of printed composite supercapacitors using anionic CNFs, PEDOT:PSS, activated carbon (AC), and carbon black (CB).[82] Here in the pilot paper production of an energy storage paper, a similar material combination was used, except in the place of anionic CNFs cationic cellulose fibers were used. Since PEDOT:PSS carries a negative charge, it adsorbed spontaneously and was retained onto the cationic fibers even after washing (Figure 19). The total amount of adsorbed PEDOT:PSS was measured using retention measurements and was found to be 0.75-1.5 wt%. To further improve retention of the other active components, such as AC, 0.2 wt% cationic polyacrylamide (CPAM) was used as a retention agent in the trials. In the

laboratory trials performed before the pilot trials, the addition of both PEDOT:PSS and AC showed the best electrochemical and electrical properties and thus were used in the pilot trials. Four separate 10-meter rolls of energy storage paper were prepared at the grammage of 100 g/m² with the composition summarized in Table 3.

Table 3. Experimental matrix for the pilot trial, with dry wt% ratios given for the formulations i, ii, iii and iv with the components cationic cellulose pulp with PEDOT:PSS (CP:PP), activated carbon (AC), carboxymethylated cellulose nanofibrils (CM-CNFs) and carbon-black dispersed by CNFs (CB:CNF). Adapted from Paper V.[121]

	Without CNF		***With CNF***	
	i		**ii**	
Without CB:CNF	CP:PP	AC	CP:PP	AC
	51.2%	48.6%	48.9%	48.6%
	CNF	CB:CNF	CNF	CB:CNF
	-	-	2.3%	-
	iii		**iv**	
With CB:CNF	CP:PP	AC	CP:PP	AC
	53.2%	45.9%	52.2%	44.6%
	CNF	CB:CNF	CNF	CB:CNF
	-	0.7%	2.3%	0.7%

All the papers showed conductivities between 1-10 S/cm. Earlier studies by Belaineh et al. have proposed that 10 wt% PEDOT:PSS is the minimum concentration required to create a conductive network between AC particles in the printed supercapacitors.[82] However, the irreversible adsorption of PEDOT:PSS onto the cationic fibers significantly reduced this threshold (1 wt% vs. 10 wt%), as shown by the detected conductivity values.

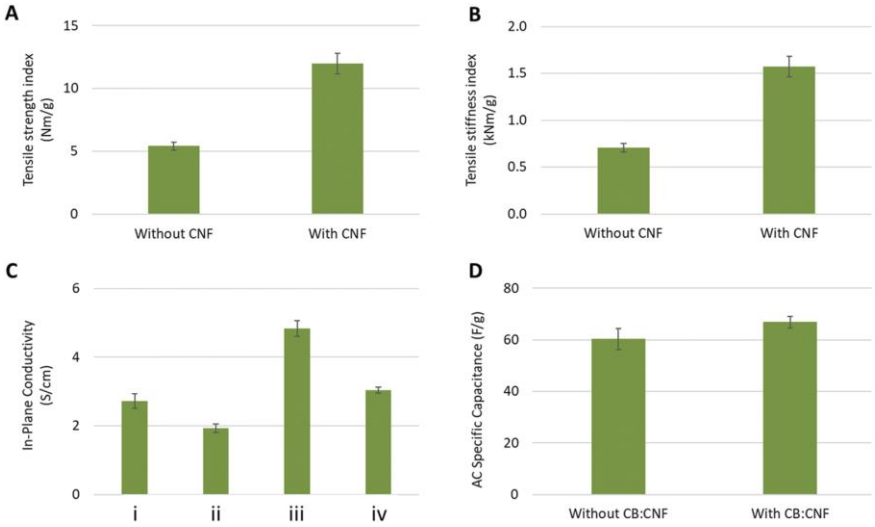

Figure 20 Effect of different additives on the paper electrode properties. The mechanical properties evaluated as tensile strength index (A), tensile stiffness index (B), the in-plane conductivity (i, ii, iii, iv refer to specific formulations that can be found in Table 3) (C), and the specific capacitance per mass unit AC (D). Adapted from Paper V.[121]

CNFs were added in the pilot trials to improve the mechanical properties of the papers. Upon the addition of CNFs both the tensile stiffness and tensile strength increased, but the electrical conductivity decreased (Figure 20a, 20b, 20c). SEM, and TGA showed that a more aggregated fiber network was created following the addition of CNF, which unfortunately also resulted in the loss of AC, and thereby decreasing the conductivity (for further details, please refer to Paper V). However, adding CB:CNF increased the electrical conductivity, since CB is a conductive filler, in addition to PEDOT:PSS.[82] The specific capacitance of the paper (with CNFs) normalized to the mass of AC was 60 F/g and was increased to 67 F/g when CB:CNF was added (Figure 20d), implying the increased accessibility of charge storage sites. Thus, the addition of CNFs did not affect the electrochemical performance but adding CB:CNF increased the capacitance.

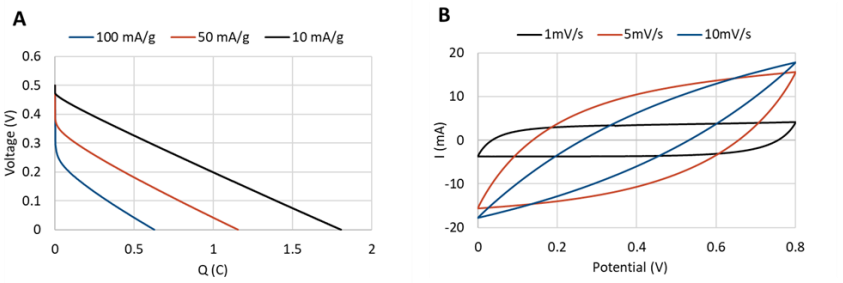

Figure 21 Characteristics of the EDLC device. (A) Discharge at different discharge currents and (B) cyclic voltammetry at different scan rates. Adapted from Paper V.[121]

To demonstrate the use of paper electrodes in energy storage devices, an EDLC (electrical double-layer capacitor) supercapacitor was assembled (Figure 4). CV and linear discharge curves (Figure 21) showed a characteristic behavior of an EDLC supercapacitor. The measured specific capacitance of 73 F/g at the discharge current of 10mA/g was comparable to commercial carbon-based supercapacitors (100 F/g). However, further improvements are needed to increase the retention of active components and mechanical properties of the formed paper electrodes. Yet, cationic fibers can significantly improve the retention of active materials for scale-up production and potentially compete with commercial supercapacitor electrodes.

5. Summary and Conclusions

The aim of the work presented in this thesis has been to improve the fundamental understanding of cellulose and conducting polymer composites, and to investigate different factors that affect the final properties of such composites.

The following conclusions can be drawn from the research described in this thesis:

1. The particle size and charge density of PEDOT:PSS complexes vary with solution parameters such as pH and ionic strength. In addition, MD simulations have shown that PEDOT:PSS has a core-shell morphology where PSS chains form a shell around the PEDOT core, and a few PSS chains can penetrate into the PEDOT rich core.

2. There is an entropic interaction between PEDOT:PSS and TEMPO- or CM-CNF, which drives the adsorption of the PEDOT:PSS to the cellulose based materials. This interaction can be controlled by different solution parameters such as pH, ionic strength and counterion type; to tailor the adsorption of PEDOT:PSS on cellulose.

3. Dialcohol modified cellulose fibers can act as a secondary dopant for PEDOT:PSS. Highly conductive, stretchable and flexible electrodes can be prepared by 3D-printing while, simultaneously, lowering the amount of PEDOT:PSS required by using fibers instead of nanocellulose. Also, supramolecular structuring of PEDOT and the simultaneous removal of PSS from the DALC/PEDOT:PSS/glycerol composites were found to be the major contributing factor behind the increased conductivity of these composites.

4. Cationic cellulose fibers can help retain CPs and conductive carbons, and may help lower the percolation threshold of the composites. The fabrication of energy storage paper, using cationic fibers on a pilot scale paper machine, demonstrates the capability of these fibers to facilitate scalable production.

In summary, this thesis addresses some of the challenges involved in the preparation of cellulose-based PEDOT:PSS composites — from understanding molecular interactions, to modification and scale-up.

6. Future Outlook

Conductive materials are required for applications such as energy storage, consumer electronics, or MedTech sensors. Cellulose based composite materials have the potential to meet this demand. However, in order to develop electrodes from cellulose composites, there is still the need for more fundamental research, new composite material and fabrication route development. This thesis takes an incremental step towards understanding the structure-property relationship between cellulose and conductive materials.

In the future, it is essential to delve deeper into the interaction between anionic polymers, conducting materials, and cellulose; using computational tools to accelerate the development of new composite materials.

The mechanism of PSS separation and removal in DALC/PEDOT:PSS composites should be studied further, both practically and through simulation. Additionally, different chemically-modified cellulose and PEDOT:PSS composites should be characterized in a similar fashion.

Lignocellulosic fibers with different chemical modifications have not been studied extensively in combination with conducting materials, with the focus instead being on nanocellulose. However, these fibers can provide further insights into the 3D structuring of conductive materials. The emphasis should be placed on selecting the best chemical modification of the fibers to improve the retention of the conductive components in the composites.

Different production methods for fiber-based devices should be explored. For example, the expertise and infrastructure available in the paper industry can be harnessed to accelerate the scale-up of cellulose based conducting electrodes, especially for energy storage applications. This will provide alternative revenue streams for the paper industry, especially those in the sector specializing in the small scale production of high value products. In addition, more extrusion-based printing techniques can be explored in order to fabricate fiber-based devices by roll-to-roll processing.

Although PEDOT:PSS has been studied in this work, the concepts developed can be extended to other electrically and ionically conducting materials, for example, conductive carbons, 2D materials, and ionic polymers. The findings can also be extrapolated to other applications, such as: fuel cells, redox flow batteries, actuators, and sensors.

7. Acknowledgements

This work would not have been possible without the support of many individuals for whom I am sincerely grateful. I would like to acknowledge:

My supervisor Prof. Lars Wågberg for allowing me to work with his team and experience the international culture. My deepest gratitude to Lars, who introduced me to the field of wood-based materials and put his trust in me even though I had no experience in this research area. Your kindness and calmness are a few qualities I admire as well as your scientific aptitude.

My co-supervisor, Dr. Per Larsson, for his invaluable discussions and support throughout the project. You are one of the most critical people I have met at KTH, which has helped me grow my scientific muscle even more. I will miss our random discussions, and I believe you are The Metal Fan! :D

My collaborators and co-authors at Digital Cellulose Centre, KTH, RISE, and Linköping University. This thesis work would not have been possible without your guidance and help. Particularly Sapiens, Mike, Emile, Göksu, Johan, Alireza, Zhen, Max Hamedi, and Torbjörn. Thank you for introducing me to the new characterization methods, valuable discussions, and guidance. I would also like to acknowledge the Treeserach platform for research infrastructure support and Vinnova for the Ph.D. funding.

All my former and current colleagues at KTH and FPT: Yunus, Kasia, Hugo, and Hailong, for all the support, discussions, and fun times in the office. I also like to thank my other colleagues: Zhaleh, Maria, Nadia, Negar, Giorgios, Johanna, and Mengxiao, for fun times at lunch and after work.

My family for their endless love and support. When life seemed hopeless, you encouraged me to get going and follow my passion. Sneha, my best friend! You have always been by my side and supported my ambitions since we first met in 2009. 13 years already and a whole life to go!

Pankaj, for your support and encouragement throughout the Ph.D. You are my inspiration, and I learn something new from you every day. Thank you for your care, love, and understanding during this challenging journey. I could not imagine a better partner. I love you!

Karishma Jain
Stockholm, November 2022

8. References

(1) Bristow, J. A.; Kolseth, P. *Paper Structure and Properties*; M. Dekker: New York, 1986.

(2) Klemm, D.; Kramer, F.; Moritz, S.; Lindström, T.; Ankerfors, M.; Gray, D.; Dorris, A. Nanocelluloses: A New Family of Nature-Based Materials. *Angewandte Chemie International Edition* **2011**, *50* (24), 5438–5466. https://doi.org/10.1002/anie.201001273.

(3) Thomas, S.; Paul, S. A.; Pothan, L. A.; Deepa, B. *Natural Fibres: Structure, Properties and Applications*. https://doi.org/10.1007/978-3-642-17370-7_1.

(4) Klemm, D.; Heublein, B.; Fink, H.-P.; Bohn, A. Cellulose: Fascinating Biopolymer and Sustainable Raw Material. *Angewandte Chemie International Edition* **2005**, *44* (22), 3358–3393. https://doi.org/10.1002/anie.200460587.

(5) Figueiredo, J. A.; Ismael, M. I.; Anjo, C. M. S.; Duarte, A. P. Cellulose and Derivatives from Wood and Fibers as Renewable Sources of Raw-Materials. In *Carbohydrates in Sustainable Development I*; Rauter, A. P., Vogel, P., Queneau, Y., Eds.; Topics in Current Chemistry; Springer: Berlin, Heidelberg, 2010; pp 117–128. https://doi.org/10.1007/128_2010_88.

(6) Gunnars, S.; Wågberg, L.; Cohen Stuart, M. A. Model Films of Cellulose: I. Method Development and Initial Results. *Cellulose* **2002**, *9* (3), 239–249. https://doi.org/10.1023/A:1021196914398.

(7) Mittal, N.; Ansari, F.; Gowda.V, K.; Brouzet, C.; Chen, P.; Larsson, P. T.; Roth, S. V.; Lundell, F.; Wågberg, L.; Kotov, N. A.; Söderberg, L. D. Multiscale Control of Nanocellulose Assembly: Transferring Remarkable Nanoscale Fibril Mechanics to Macroscale Fibers. *ACS Nano* **2018**, *12* (7), 6378–6388. https://doi.org/10.1021/acsnano.8b01084.

(8) Saito, T.; Kuramae, R.; Wohlert, J.; Berglund, L. A.; Isogai, A. An Ultrastrong Nanofibrillar Biomaterial: The Strength of Single Cellulose Nanofibrils

Revealed via Sonication-Induced Fragmentation. *Biomacromolecules* **2013**, *14* (1), 248–253. https://doi.org/10.1021/bm301674e.

(9) Gibson, L. J. The Hierarchical Structure and Mechanics of Plant Materials. *Journal of The Royal Society Interface* **2012**, *9* (76), 2749–2766. https://doi.org/10.1098/rsif.2012.0341.

(10) Sakurada, I.; Nukushina, Y.; Ito, T. Experimental Determination of the Elastic Modulus of Crystalline Regions in Oriented Polymers. *Journal of Polymer Science* **1962**, *57* (165), 651–660. https://doi.org/10.1002/pol.1962.1205716551.

(11) Turbak, A. F.; Snyder, F. W. MICROFIBRILLATEDCELLULOSE,A N E WCELLULOSE PRODUCT:PROPERTIES,USES,ANDCOMMERCIAL POTENTIAL. 13.

(12) Herrick, F. W.; Casebier, R. L.; Hamilton, J. K.; Sandberg, K. R. Microfibrillated Cellulose: Morphology and Accessibility. *J. Appl. Polym. Sci.: Appl. Polym. Symp.; (United States)* **1983**, *37*.

(13) Saito, T.; Hirota, M.; Tamura, N.; Kimura, S.; Fukuzumi, H.; Heux, L.; Isogai, A. Individualization of Nano-Sized Plant Cellulose Fibrils by Direct Surface Carboxylation Using TEMPO Catalyst under Neutral Conditions. *Biomacromolecules* **2009**, *10* (7), 1992–1996. https://doi.org/10.1021/bm900414t.

(14) Gorur, Y. C.; Larsson, P. A.; Wågberg, L. Self-Fibrillating Cellulose Fibers: Rapid In Situ Nanofibrillation to Prepare Strong, Transparent, and Gas Barrier Nanopapers. *Biomacromolecules* **2020**, *21* (4), 1480–1488. https://doi.org/10.1021/acs.biomac.0c00040.

(15) Li, T.; Chen, C.; Brozena, A. H.; Zhu, J. Y.; Xu, L.; Driemeier, C.; Dai, J.; Rojas, O. J.; Isogai, A.; Wågberg, L.; Hu, L. Developing Fibrillated Cellulose as a Sustainable Technological Material. *Nature* **2021**, *590* (7844), 47–56. https://doi.org/10.1038/s41586-020-03167-7.

(16) Fall, A. B.; Lindström, S. B.; Sundman, O.; Ödberg, L.; Wågberg, L. Colloidal Stability of Aqueous Nanofibrillated Cellulose Dispersions. *Langmuir* **2011**, *27* (18), 11332–11338. https://doi.org/10.1021/la201947x.

(17) Johan Foster, E.; J. Moon, R.; P. Agarwal, U.; J. Bortner, M.; Bras, J.; Camarero-Espinosa, S.; J. Chan, K.; D. Clift, M. J.; D. Cranston, E.; J. Eichhorn, S.; M. Fox, D.; Y. Hamad, W.; Heux, L.; Jean, B.; Korey, M.; Nieh, W.; J. Ong, K.; S. Reid, M.; Renneckar, S.; Roberts, R.; Anne Shatkin, J.; Simonsen, J.; Stinson-Bagby, K.; Wanasekara, N.; Youngblood, J. Current Characterization Methods for Cellulose Nanomaterials. *Chemical Society Reviews* **2018**, *47* (8), 2609–2679. https://doi.org/10.1039/C6CS00895J.

(18) Xu, X.; Liu, F.; Jiang, L.; Zhu, J. Y.; Haagenson, D.; Wiesenborn, D. P. Cellulose Nanocrystals vs. Cellulose Nanofibrils: A Comparative Study on Their Microstructures and Effects as Polymer Reinforcing Agents. *ACS Appl. Mater. Interfaces* **2013**, *5* (8), 2999–3009. https://doi.org/10.1021/am302624t.

(19) Onwukamike, K. N.; Grelier, S.; Grau, E.; Cramail, H.; Meier, M. A. R. Critical Review on Sustainable Homogeneous Cellulose Modification: Why Renewability Is Not Enough. *ACS Sustainable Chem. Eng.* **2019**, *7* (2), 1826–1840. https://doi.org/10.1021/acssuschemeng.8b04990.

(20) Jedvert, K.; Heinze, T. Cellulose Modification and Shaping – a Review. *Journal of Polymer Engineering* **2017**, *37* (9), 845–860. https://doi.org/10.1515/polyeng-2016-0272.

(21) Walecka, J. A. AN INVESTIGATION OF LOW DEGREE OF SUBSTITUTION CARBOXYMETHYLCELLULOSES. 117.

(22) Wågberg, L.; Winter, L.; Ödberg, L.; Lindström, T. On the Charge Stoichiometry upon Adsorption of a Cationic Polyelectrolyte on Cellulosic Materials. *Colloids and Surfaces* **1987**, *27* (4), 163–173. https://doi.org/10.1016/0166-6622(87)80140-3.

(23) Shimizu, M.; Fukuzumi, H.; Saito, T.; Isogai, A. Preparation and Characterization of TEMPO-Oxidized Cellulose Nanofibrils with Ammonium

Carboxylate Groups. *International Journal of Biological Macromolecules* **2013**, *59*, 99–104. https://doi.org/10.1016/j.ijbiomac.2013.04.021.

(24) Saito, T.; Kimura, S.; Nishiyama, Y.; Isogai, A. Cellulose Nanofibers Prepared by TEMPO-Mediated Oxidation of Native Cellulose. *Biomacromolecules* **2007**, *8* (8), 2485–2491. https://doi.org/10.1021/bm0703970.

(25) Kim, U.-J.; Kuga, S.; Wada, M.; Okano, T.; Kondo, T. Periodate Oxidation of Crystalline Cellulose. *Biomacromolecules* **2000**, *1* (3), 488–492. https://doi.org/10.1021/bm0000337.

(26) Nypelö, T.; Berke, B.; Spirk, S.; Sirviö, J. A. Review: Periodate Oxidation of Wood Polysaccharides—Modulation of Hierarchies. *Carbohydrate Polymers* **2021**, *252*, 117105. https://doi.org/10.1016/j.carbpol.2020.117105.

(27) Larsson, P.; RE, G. L. Melt-Processed Material with High Cellulose Fiber Content. US20190382508A1, December 19, 2019.

(28) Larsson, P. A.; Wågberg, L. Towards Natural-Fibre-Based Thermoplastic Films Produced by Conventional Papermaking. *Green Chem.* **2016**, *18* (11), 3324–3333. https://doi.org/10.1039/C5GC03068D.

(29) Larsson, P. A.; Berglund, L. A.; Wågberg, L. Ductile All-Cellulose Nanocomposite Films Fabricated from Core–Shell Structured Cellulose Nanofibrils. *Biomacromolecules* **2014**, *15* (6), 2218–2223. https://doi.org/10.1021/bm500360c.

(30) Larsson, P. A.; Berglund, L. A.; Wågberg, L. Highly Ductile Fibres and Sheets by Core-Shell Structuring of the Cellulose Nanofibrils. *Cellulose* **2014**, *21* (1), 323–333. https://doi.org/10.1007/s10570-013-0099-9.

(31) Whistler, R. L.; BeMiller, J. N. *Starch: Chemistry and Technology*, 3rd ed.; Food science and technology, International Series; Academic Press: London, 2009.

(32) Pei, A.; Butchosa, N.; A. Berglund, L.; Zhou, Q. Surface Quaternized Cellulose Nanofibrils with High Water Absorbency and Adsorption Capacity for

Anionic Dyes. *Soft Matter* **2013**, *9* (6), 2047–2055. https://doi.org/10.1039/C2SM27344F.

(33) Chiang, C. K.; Fincher, C. R.; Park, Y. W.; Heeger, A. J.; Shirakawa, H.; Louis, E. J.; Gau, S. C.; MacDiarmid, A. G. Electrical Conductivity in Doped Polyacetylene. *Phys. Rev. Lett.* **1977**, *39* (17), 1098–1101. https://doi.org/10.1103/PhysRevLett.39.1098.

(34) Shirakawa, H.; Louis, E. J.; MacDiarmid, A. G.; Chiang, C. K.; Heeger, A. J. Synthesis of Electrically Conducting Organic Polymers: Halogen Derivatives of Polyacetylene, (CH). *J. Chem. Soc., Chem. Commun.* **1977**, No. 16, 578–580. https://doi.org/10.1039/C39770000578.

(35) Elschner, A.; Kirchmeyer, S.; Lovenich, W.; Merker, U.; Reuter, K.; Kirchmeyer, S.; Lovenich, W.; Merker, U.; Reuter, K. *PEDOT : Principles and Applications of an Intrinsically Conductive Polymer*; CRC Press, 2010. https://doi.org/10.1201/b10318.

(36) Skotheim, T. A. *Handbook of Conducting Polymers, Second Edition,*; CRC Press, 1997.

(37) Bredas, J. L.; Street, G. B. Polarons, Bipolarons, and Solitons in Conducting Polymers. *Acc. Chem. Res.* **1985**, *18* (10), 309–315. https://doi.org/10.1021/ar00118a005.

(38) Sun, K.; Zhang, S.; Li, P.; Xia, Y.; Zhang, X.; Du, D.; Isikgor, F. H.; Ouyang, J. Review on Application of PEDOTs and PEDOT:PSS in Energy Conversion and Storage Devices. *J Mater Sci: Mater Electron* **2015**, *26* (7), 4438–4462. https://doi.org/10.1007/s10854-015-2895-5.

(39) Bhat, M. A.; Rather, R. A.; Shalla, A. H. PEDOT and PEDOT:PSS Conducting Polymeric Hydrogels: A Report on Their Emerging Applications. *Synthetic Metals* **2021**, *273*, 116709. https://doi.org/10.1016/j.synthmet.2021.116709.

(40) Mokhtar, S. M. A.; Eulate, E. A. de; Yamada, M.; Prow, T. W.; Evans, D. R. Conducting Polymers in Wearable Devices. *MEDICAL DEVICES & SENSORS* **2021**, *4* (1), e10160. https://doi.org/10.1002/mds3.10160.

(41) Guo, X.; Facchetti, A. The Journey of Conducting Polymers from Discovery to Application. *Nat. Mater.* **2020**, *19* (9), 922–928. https://doi.org/10.1038/s41563-020-0778-5.

(42) Wen, Y.; Xu, J. Scientific Importance of Water-Processable PEDOT–PSS and Preparation, Challenge and New Application in Sensors of Its Film Electrode: A Review. *Journal of Polymer Science Part A: Polymer Chemistry* **2017**, *55* (7), 1121–1150. https://doi.org/10.1002/pola.28482.

(43) Modarresi, M.; Felipe Franco-Gonzalez, J.; Zozoulenko, I. Morphology and Ion Diffusion in PEDOT:Tos. A Coarse Grained Molecular Dynamics Simulation. *Physical Chemistry Chemical Physics* **2018**, *20* (25), 17188–17198. https://doi.org/10.1039/C8CP02902D.

(44) Groenendaal, B. L.; Jonas, F.; Freitag, D.; Pielartzik, H.; Reynolds, J. R. PEDOT and Its Derivatives; Past, Present, and Future. *Adv. Mater.* **2000**, *7*, 481–494.

(45) Gueye, M. N.; Carella, A.; Faure-Vincent, J.; Demadrille, R.; Simonato, J.-P. Progress in Understanding Structure and Transport Properties of PEDOT-Based Materials: A Critical Review. *Progress in Materials Science* **2020**, *108*, 100616. https://doi.org/10.1016/j.pmatsci.2019.100616.

(46) Hofmann, A. I.; Katsigiannopoulos, D.; Mumtaz, M.; Petsagkourakis, I.; Pecastaings, G.; Fleury, G.; Schatz, C.; Pavlopoulou, E.; Brochon, C.; Hadziioannou, G.; Cloutet, E. *How To Choose Polyelectrolytes for Aqueous Dispersions of Conducting PEDOT Complexes*. https://pubs.acs.org/doi/abs/10.1021/acs.macromol.6b02504 (accessed 2020-04-12). https://doi.org/10.1021/acs.macromol.6b02504.

(47) Gangopadhyay, R.; Das, B.; Molla, M. R. How Does PEDOT Combine with PSS? Insights from Structural Studies. *RSC Adv.* **2014**, *4* (83), 43912–43920. https://doi.org/10.1039/C4RA08666J.

(48) Horii, T.; Li, Y.; Mori, Y.; Okuzaki, H. Correlation between the Hierarchical Structure and Electrical Conductivity of PEDOT/PSS. *Polym J* **2015**, *47* (10), 695–699. https://doi.org/10.1038/pj.2015.48.

(49) Mochizuki, Y.; Horii, T.; Okuzaki, H. Effect of PH on Structure and Conductivity of PEDOT/PSS. *Trans. Mat. Res. Soc. Japan* **2012**, *37* (2), 307–310. https://doi.org/10.14723/tmrsj.37.307.

(50) Xia, Y.; Ouyang, J. Anion Effect on Salt-Induced Conductivity Enhancement of Poly(3,4-Ethylenedioxythiophene):Poly(Styrenesulfonate) Films. *Organic Electronics* **2010**, *11* (6), 1129–1135. https://doi.org/10.1016/j.orgel.2010.04.007.

(51) Ouyang, L.; Musumeci, C.; Jafari, M. J.; Ederth, T.; Inganäs, O. Imaging the Phase Separation Between PEDOT and Polyelectrolytes During Processing of Highly Conductive PEDOT:PSS Films. *ACS Appl. Mater. Interfaces* **2015**, *7* (35), 19764–19773. https://doi.org/10.1021/acsami.5b05439.

(52) Crispin, X.; Jakobsson, F. L. E.; Crispin, A.; Grim, P. C. M.; Andersson, P.; Volodin, A.; van Haesendonck, C. The Origin of the High Conductivity of Poly(3,4-Ethylenedioxythiophene)-Poly(Styrenesulfonate) (PEDOT-PSS) Plastic Electrodes. 7.

(53) Fan, X.; Nie, W.; Tsai, H.; Wang, N.; Huang, H.; Cheng, Y.; Wen, R.; Ma, L.; Yan, F.; Xia, Y. PEDOT:PSS for Flexible and Stretchable Electronics: Modifications, Strategies, and Applications. *Adv. Sci.* **2019**, *6* (19), 1900813. https://doi.org/10.1002/advs.201900813.

(54) Ouyang, J. "Secondary Doping" Methods to Significantly Enhance the Conductivity of PEDOT:PSS for Its Application as Transparent Electrode of Optoelectronic Devices. *Displays* **2013**, *34* (5), 423–436. https://doi.org/10.1016/j.displa.2013.08.007.

(55) *Salt-Induced Charge Screening and Significant Conductivity Enhancement of Conducting Poly(3,4-ethylenedioxythiophene):Poly(styrenesulfonate) | Macromolecules*. https://pubs.acs.org/doi/abs/10.1021/ma900327d (accessed 2020-04-29).

(56) Rudd, S.; Evans, D. Recent Advances in the Aqueous Applications of PEDOT. *Nanoscale Advances* **2022**, *4* (3), 733–741. https://doi.org/10.1039/D1NA00748C.

(57) Wang, Z.; Lee, Y.-H.; Kim, S.-W.; Seo, J.-Y.; Lee, S.-Y.; Nyholm, L. Why Cellulose-Based Electrochemical Energy Storage Devices? *Advanced Materials n/a* (n/a), 2000892. https://doi.org/10.1002/adma.202000892.

(58) Wang, G.; Zhang, L.; Zhang, J. A Review of Electrode Materials for Electrochemical Supercapacitors. *Chem. Soc. Rev.* **2012**, *41* (2), 797–828. https://doi.org/10.1039/C1CS15060J.

(59) Dhandapani, E.; Thangarasu, S.; Ramesh, S.; Ramesh, K.; Vasudevan, R.; Duraisamy, N. Recent Development and Prospective of Carbonaceous Material, Conducting Polymer and Their Composite Electrode Materials for Supercapacitor — A Review. *Journal of Energy Storage* **2022**, *52*, 104937. https://doi.org/10.1016/j.est.2022.104937.

(60) Mei, B.-A.; Munteshari, O.; Lau, J.; Dunn, B.; Pilon, L. Physical Interpretations of Nyquist Plots for EDLC Electrodes and Devices. *J. Phys. Chem. C* **2018**, *122* (1), 194–206. https://doi.org/10.1021/acs.jpcc.7b10582.

(61) Tobjörk, D.; Österbacka, R. Paper Electronics. *Advanced Materials* **2011**, *23* (17), 1935–1961. https://doi.org/10.1002/adma.201004692.

(62) Abas, Z.; Kim, H. S.; Kim, J.; Kim, J.-H. Cellulose Electro-Active Paper: From Discovery to Technology Applications. *Frontiers in Materials* **2014**, *1*.

(63) Françon, H.; Wang, Z.; Marais, A.; Mystek, K.; Piper, A.; Granberg, H.; Malti, A.; Gatenholm, P.; Larsson, P. A.; Wågberg, L. Ambient-Dried, 3D-Printable and Electrically Conducting Cellulose Nanofiber Aerogels by Inclusion of

Functional Polymers. *Advanced Functional Materials* **2020**, *30* (12), 1909383. https://doi.org/10.1002/adfm.201909383.

(64) Fou, A. C.; Rubner, M. F. Molecular-Level Processing of Conjugated Polymers. 2. Layer-by-Layer Manipulation of In-Situ Polymerized p-Type Doped Conducting Polymers. *Macromolecules* **1995**, *28* (21), 7115–7120. https://doi.org/10.1021/ma00125a013.

(65) Nyström, G.; Mihranyan, A.; Razaq, A.; Lindström, T.; Nyholm, L.; Strømme, M. A Nanocellulose Polypyrrole Composite Based on Microfibrillated Cellulose from Wood. *J. Phys. Chem. B* **2010**, *114* (12), 4178–4182. https://doi.org/10.1021/jp911272m.

(66) Gopakumar, D. A.; Pai, A. R.; Pottathara, Y. B.; Pasquini, D.; Carlos de Morais, L.; Luke, M.; Kalarikkal, N.; Grohens, Y.; Thomas, S. Cellulose Nanofiber-Based Polyaniline Flexible Papers as Sustainable Microwave Absorbers in the X-Band. *ACS Appl. Mater. Interfaces* **2018**, *10* (23), 20032–20043. https://doi.org/10.1021/acsami.8b04549.

(67) Gopakumar, D. A.; Pai, A. R.; Pottathara, Y. B.; Pasquini, D.; de Morais, L. C.; Khalil H.P.S., A.; Nzihou, A.; Thomas, S. Flexible Papers Derived from Polypyrrole Deposited Cellulose Nanofibers for Enhanced Electromagnetic Interference Shielding in Gigahertz Frequencies. *Journal of Applied Polymer Science* **2021**, *138* (16), 50262. https://doi.org/10.1002/app.50262.

(68) Hsu, H. H.; Khosrozadeh, A.; Li, B.; Luo, G.; Xing, M.; Zhong, W. An Eco-Friendly, Nanocellulose/RGO/in Situ Formed Polyaniline for Flexible and Free-Standing Supercapacitors. *ACS Sustainable Chem. Eng.* **2019**, *7* (5), 4766–4776. https://doi.org/10.1021/acssuschemeng.8b04947.

(69) Kelly, F. M.; Johnston, J. H.; Borrmann, T.; Richardson, M. J. Functionalised Hybrid Materials of Conducting Polymers with Individual Fibres of Cellulose. *European Journal of Inorganic Chemistry* **2007**, *2007* (35), 5571–5577. https://doi.org/10.1002/ejic.200700608.

(70) Sapurina, I.; Kazantseva, N. E.; Ryvkina, N. G.; Prokeš, J.; Sáha, P.; Stejskal, J. Electromagnetic Radiation Shielding by Composites of Conducting Polymers and Wood. *Journal of Applied Polymer Science* **2005**, *95* (4), 807–814. https://doi.org/10.1002/app.21240.

(71) Lay, M.; Pèlach, M. À.; Pellicer, N.; Tarrés, J. A.; Bun, K. N.; Vilaseca, F. Smart Nanopaper Based on Cellulose Nanofibers with Hybrid PEDOT:PSS/Polypyrrole for Energy Storage Devices. *Carbohydrate Polymers* **2017**, *165*, 86–95. https://doi.org/10.1016/j.carbpol.2017.02.043.

(72) Sasso, C.; Zeno, E.; Petit-Conil, M.; Chaussy, D.; Belgacem, M. N.; Tapin-Lingua, S.; Beneventi, D. Highly Conducting Polypyrrole/Cellulose Nanocomposite Films with Enhanced Mechanical Properties. *Macromolecular Materials and Engineering* **2010**, *295* (10), 934–941. https://doi.org/10.1002/mame.201000148.

(73) Qian, X.; Shen, J.; Yu, G.; An, X. INFLUENCE OF PULP FIBER SUBSTRATE ON CONDUCTIVITY OF POLYANILINE-COATED CONDUCTIVE PAPER PREPARED BY IN-SITU POLYMERIZATION. 9.

(74) Wistrand, I.; Lingström, R.; Wågberg, L. Preparation of Electrically Conducting Cellulose Fibres Utilizing Polyelectrolyte Multilayers of Poly(3,4-Ethylenedioxythiophene):Poly(Styrene Sulphonate) and Poly(Allyl Amine). *European Polymer Journal* **2007**, *43* (10), 4075–4091. https://doi.org/10.1016/j.eurpolymj.2007.03.053.

(75) Zheng, Z.; McDonald, J.; Khillan, R.; Su, Y.; Shutava, T.; Grozdits, G.; Lvov, Y. M. Layer-by-Layer Nanocoating of Lignocellulose Fibers for Enhanced Paper Properties. *Journal of Nanoscience and Nanotechnology* **2006**, *6* (3), 624–632. https://doi.org/10.1166/jnn.2006.081.

(76) Agarwal, M.; Lvov, Y.; Varahramyan, K. Conductive Wood Microfibres for Smart Paper through Layer-by-Layer Nanocoating. *Nanotechnology* **2006**, *17* (21), 5319–5325. https://doi.org/10.1088/0957-4484/17/21/006.

(77) Montibon, E.; Järnström, L.; Lestelius, M. Characterization of Poly(3,4-Ethylenedioxythiophene)/Poly(Styrene Sulfonate) (PEDOT:PSS) Adsorption on Cellulosic Materials. *Cellulose* **2009**, *16* (5), 807–815. https://doi.org/10.1007/s10570-009-9303-3.

(78) Montibon, E.; Lestelius, M.; Järnström, L. Electroconductive Paper Prepared by Coating with Blends of Poly(3,4-Ethylenedioxythiophene)/Poly(4-Styrenesulfonate) and Organic Solvents. *Journal of Applied Polymer Science* **2010**, *117* (6), 3524–3532. https://doi.org/10.1002/app.32250.

(79) Malti, A.; Edberg, J.; Granberg, H.; Khan, Z. U.; Andreasen, J. W.; Liu, X.; Zhao, D.; Zhang, H.; Yao, Y.; Brill, J. W.; Engquist, I.; Fahlman, M.; Wågberg, L.; Crispin, X.; Berggren, M. An Organic Mixed Ion-Electron Conductor for Power Electronics. *Adv. Sci.* **2016**, *3* (2), 1500305. https://doi.org/10.1002/advs.201500305.

(80) Edberg, J.; Malti, A.; Granberg, H.; Hamedi, M. M.; Crispin, X.; Engquist, I.; Berggren, M. Electrochemical Circuits from 'Cut and Stick' PEDOT:PSS-Nanocellulose Composite. *Flex. Print. Electron.* **2017**, *2* (4), 045010. https://doi.org/10.1088/2058-8585/aa8027.

(81) Belaineh, D.; Andreasen, J. W.; Palisaitis, J.; Malti, A.; Håkansson, K.; Wågberg, L.; Crispin, X.; Engquist, I.; Berggren, M. Controlling the Organization of PEDOT:PSS on Cellulose Structures. *ACS Appl. Polym. Mater.* **2019**, *1* (9), 2342–2351. https://doi.org/10.1021/acsapm.9b00444.

(82) Belaineh, D.; Brooke, R.; Sani, N.; Say, M. G.; Håkansson, K. M. O.; Engquist, I.; Berggren, M.; Edberg, J. Printable Carbon-Based Supercapacitors Reinforced with Cellulose and Conductive Polymers. *Journal of Energy Storage* **2022**, *50*, 104224. https://doi.org/10.1016/j.est.2022.104224.

(83) Hoeng, F.; Denneulin, A.; Bras, J. Use of Nanocellulose in Printed Electronics: A Review. *Nanoscale* **2016**, *8* (27), 13131–13154. https://doi.org/10.1039/C6NR03054H.

(84) Brooke, R.; Lay, M.; Jain, K.; Francon, H.; Say, M. G.; Belaineh, D.; Wang, X.; Håkansson, K. M. O.; Wågberg, L.; Engquist, I.; Edberg, J.; Berggren, M. Nanocellulose and PEDOT:PSS Composites and Their Applications. *Polymer Reviews* **2022**, *0* (0), 1–41. https://doi.org/10.1080/15583724.2022.2106491.

(85) Mehandzhiyski, A. Y.; Zozoulenko, I. Computational Microscopy of PEDOT:PSS/Cellulose Composite Paper. *ACS Appl. Energy Mater.* **2019**, *2* (5), 3568–3577. https://doi.org/10.1021/acsaem.9b00307.

(86) Zhou, J.; Hsieh, Y.-L. Conductive Polymer Protonated Nanocellulose Aerogels for Tunable and Linearly Responsive Strain Sensors. *ACS Appl. Mater. Interfaces* **2018**, *10* (33), 27902–27910. https://doi.org/10.1021/acsami.8b10239.

(87) Hamedi, M. M.; Hajian, A.; Fall, A. B.; Håkansson, K.; Salajkova, M.; Lundell, F.; Wågberg, L.; Berglund, L. A. Highly Conducting, Strong Nanocomposites Based on Nanocellulose-Assisted Aqueous Dispersions of Single-Wall Carbon Nanotubes. *ACS Nano* **2014**, *8* (3), 2467–2476. https://doi.org/10.1021/nn4060368.

(88) Hajian, A.; Lindström, S. B.; Pettersson, T.; Hamedi, M. M.; Wågberg, L. Understanding the Dispersive Action of Nanocellulose for Carbon Nanomaterials. *Nano Lett.* **2017**, *17* (3), 1439–1447. https://doi.org/10.1021/acs.nanolett.6b04405.

(89) Salajkova, M.; Valentini, L.; Zhou, Q.; Berglund, L. A. Tough Nanopaper Structures Based on Cellulose Nanofibers and Carbon Nanotubes. *Composites Science and Technology* **2013**, *87*, 103–110. https://doi.org/10.1016/j.compscitech.2013.06.014.

(90) Françon, H. S.; Gorur, Y. C.; Montanari, C.; Larsson, P. A.; Wågberg, L. Toward Li-Ion Graphite Anodes with Enhanced Mechanical and Electrochemical Properties Using Binders from Chemically Modified Cellulose Fibers. *ACS Appl. Energy Mater.* **2022**, acsaem.2c00525. https://doi.org/10.1021/acsaem.2c00525.

(91) Gorur, Y. C.; Francon, H. S.; Sethi, J.; Maddalena, L.; Montanari, C.; Reid, M. S.; Erlandsson, J.; Carosio, F.; Larsson, P. A.; Wågberg, L. Rapidly Prepared

Nanocellulose Hybrids as Gas Barrier, Flame Retardant, and Energy Storage Materials. *ACS Appl. Nano Mater.* **2022**. https://doi.org/10.1021/acsanm.2c01530.

(92) Miyashiro, D.; Hamano, R.; Umemura, K. A Review of Applications Using Mixed Materials of Cellulose, Nanocellulose and Carbon Nanotubes. *Nanomaterials* **2020**, *10* (2), 186. https://doi.org/10.3390/nano10020186.

(93) Katz, S.; Beatson, R. P.; Anthony, M. S. The Determination of Strong and Weak Acidic Groups in Sulfite Pulps. *Svensk Papperstidning-nordisk Cellulosa* **1984**. https://doi.org/null.

(94) Jain, K.; Mehandzhiyski, A. Y.; Zozoulenko, I.; Wågberg, L. PEDOT:PSS Nano-Particles in Aqueous Media: A Comparative Experimental and Molecular Dynamics Study of Particle Size, Morphology and z-Potential. *Journal of Colloid and Interface Science* **2021**, *584*, 57–66. https://doi.org/10.1016/j.jcis.2020.09.070.

(95) Takano, T.; Masunaga, H.; Fujiwara, A.; Okuzaki, H.; Sasaki, T. PEDOT Nanocrystal in Highly Conductive PEDOT:PSS Polymer Films. *Macromolecules* **2012**, *45* (9), 3859–3865. https://doi.org/10.1021/ma300120g.

(96) Yan, H.; Arima, S.; Mori, Y.; Kagata, T.; Sato, H.; Okuzaki, H. Poly(3,4-Ethylenedioxythiophene)/Poly(4-Styrenesulfonate): Correlation between Colloidal Particles and Thin Films. *Thin Solid Films* **2009**, *517* (11), 3299–3303. https://doi.org/10.1016/j.tsf.2009.01.004.

(97) Kemerink, M.; Timpanaro, S.; de Kok, M. M.; Meulenkamp, E. A.; Touwslager, F. J. Three-Dimensional Inhomogeneities in PEDOT:PSS Films. *J. Phys. Chem. B* **2004**, *108* (49), 18820–18825. https://doi.org/10.1021/jp0464674.

(98) Kok, M. M. de; Buechel, M.; Vulto, S. I. E.; Weijer, P. van de; Meulenkamp, E. A.; Winter, S. H. P. M. de; Mank, A. J. G.; Vorstenbosch, H. J. M.; Weijtens, C. H. L.; Elsbergen, V. van. Modification of PEDOT:PSS as Hole Injection Layer in

Polymer LEDs. *physica status solidi (a)* **2004**, *201* (6), 1342–1359. https://doi.org/10.1002/pssa.200404338.

(99) Weijtens, C. H. L.; van Elsbergen, V.; de Kok, M. M.; de Winter, S. H. P. M. Effect of the Alkali Metal Content on the Electronic Properties of PEDOT:PSS. *Organic Electronics* **2005**, *6* (2), 97–104. https://doi.org/10.1016/j.orgel.2005.02.005.

(100) Sauerbrey, G. Verwendung von Schwingquarzen Zur Wägung Dünner Schichten Und Zur Mikrowägung. *Zeitschrift für Physik* **1959**, *155* (2), 206–222. https://doi.org/10.1007/BF01337937.

(101) Jain, K.; Reid, M. S.; Larsson, P. A.; Wågberg, L. On the Interaction Between Pedot:Pss and Cellulose: Adsorption Mechanisms and Controlling Factors. *Carbohydrate Polymers* **2021**, *260*, 117818. https://doi.org/10.1016/j.carbpol.2021.117818.

(102) Fu, J.; Schlenoff, J. B. Driving Forces for Oppositely Charged Polyion Association in Aqueous Solutions: Enthalpic, Entropic, but Not Electrostatic. *J. Am. Chem. Soc.* **2016**, *138* (3), 980–990. https://doi.org/10.1021/jacs.5b11878.

(103) Wådgberg, L.; Odberg, L.; Glad-Nordmark, G. Charge Determination of Porous Substrates by Polyelectrolyte Adsorption: Part 1. Carboxymethylated, Bleached Cellulosic Fibers. *Nordic Pulp & Paper Research Journal* **1989**, *4* (2), 71–76. https://doi.org/10.3183/npprj-1989-04-02-p071-076.

(104) Tiraferri, A.; Maroni, P.; Borkovec, M. Adsorption of Polyelectrolytes to Like-Charged Substrates Induced by Multivalent Counterions as Exemplified by Poly(Styrene Sulfonate) and Silica. *Phys. Chem. Chem. Phys.* **2015**, *17* (16), 10348–10352. https://doi.org/10.1039/C5CP00910C.

(105) Turesson, M.; Labbez, C.; Nonat, A. Calcium Mediated Polyelectrolyte Adsorption on Like-Charged Surfaces. *Langmuir* **2011**, *27* (22), 13572–13581. https://doi.org/10.1021/la2030846.

(106) Benselfelt, T.; Nordenström, M.; Hamedi, M. M.; Wågberg, L. Ion-Induced Assemblies of Highly Anisotropic Nanoparticles Are Governed by Ion–Ion

Correlation and Specific Ion Effects. *Nanoscale* **2019**, *11* (8), 3514–3520. https://doi.org/10.1039/C8NR10175B.

(107) He, H.; Zhang, L.; Yue, S.; Yu, S.; Wei, J.; Ouyang, J. Enhancement in the Mechanical Stretchability of PEDOT:PSS Films by Compounds of Multiple Hydroxyl Groups for Their Application as Transparent Stretchable Conductors. *Macromolecules* **2021**, *54* (3), 1234–1242. https://doi.org/10.1021/acs.macromol.0c02309.

(108) He, H.; Ouyang, J. Enhancements in the Mechanical Stretchability and Thermoelectric Properties of PEDOT:PSS for Flexible Electronics Applications. *Acc. Mater. Res.* **2020**, *1* (2), 146–157. https://doi.org/10.1021/accountsmr.0c00021.

(109) Snook, G. A.; Kao, P.; Best, A. S. Conducting-Polymer-Based Supercapacitor Devices and Electrodes. *Journal of Power Sources* **2011**, *196* (1), 1–12. https://doi.org/10.1016/j.jpowsour.2010.06.084.

(110) Chou, T.-R.; Chen, S.-H.; Chiang, Y.-T.; Lin, Y.-T.; Chao, C.-Y. Highly Conductive PEDOT:PSS Films by Post-Treatment with Dimethyl Sulfoxide for ITO-Free Liquid Crystal Display. *J. Mater. Chem. C* **2015**, *3* (15), 3760–3766. https://doi.org/10.1039/C5TC00276A.

(111) Ouyang, J.; Xu, Q.; Chu, C.-W.; Yang, Y.; Li, G.; Shinar, J. On the Mechanism of Conductivity Enhancement in Poly(3,4-Ethylenedioxythiophene):Poly(Styrene Sulfonate) Film through Solvent Treatment. *Polymer* **2004**, *45* (25), 8443–8450. https://doi.org/10.1016/j.polymer.2004.10.001.

(112) Duc, C.; Vlandas, A.; Malliaras, G. G.; Senez, V. Wettability of PEDOT:PSS Films. *Soft Matter* **2016**, *12* (23), 5146–5153. https://doi.org/10.1039/C6SM00599C.

(113) Crispin, X.; Marciniak, S.; Osikowicz, W.; Zotti, G.; van der Gon, A. W. D.; Louwet, F.; Fahlman, M.; Groenendaal, L.; De Schryver, F.; Salaneck, W. R. Conductivity, Morphology, Interfacial Chemistry, and Stability of Poly(3,4-

Ethylene Dioxythiophene)–Poly(Styrene Sulfonate): A Photoelectron Spectroscopy Study. *Journal of Polymer Science Part B: Polymer Physics* **2003**, *41* (21), 2561–2583. https://doi.org/10.1002/polb.10659.

(114) Palumbiny, C. M.; Liu, F.; Russell, T. P.; Hexemer, A.; Wang, C.; Müller-Buschbaum, P. The Crystallization of PEDOT:PSS Polymeric Electrodes Probed In Situ during Printing. *Advanced Materials* **2015**, *27* (22), 3391–3397. https://doi.org/10.1002/adma.201500315.

(115) Kim, S.-M.; Kim, C.-H.; Kim, Y.; Kim, N.; Lee, W.-J.; Lee, E.-H.; Kim, D.; Park, S.; Lee, K.; Rivnay, J.; Yoon, M.-H. Influence of PEDOT:PSS Crystallinity and Composition on Electrochemical Transistor Performance and Long-Term Stability. *Nat Commun* **2018**, *9* (1), 3858. https://doi.org/10.1038/s41467-018-06084-6.

(116) Moraes, M. R.; Alves, A. C.; Toptan, F.; Martins, M. S.; Vieira, E. M. F.; Paleo, A. J.; Souto, A. P.; Santos, W. L. F.; Esteves, M. F.; Zille, A. Glycerol/PEDOT:PSS Coated Woven Fabric as a Flexible Heating Element on Textiles. *J. Mater. Chem. C* **2017**, *5* (15), 3807–3822. https://doi.org/10.1039/C7TC00486A.

(117) Migliaccio, L.; Altamura, D.; Scattarella, F.; Giannini, C.; Manini, P.; Gesuele, F.; Maglione, M. G.; Tassini, P.; Pezzella, A. Impact of Eumelanin–PEDOT Blending: Increased PEDOT Crystalline Order and Packing–Conductivity Relationship in Ternary PEDOT:PSS:Eumelanin Thin Films. *Advanced Electronic Materials* **2019**, *5* (3), 1800585. https://doi.org/10.1002/aelm.201800585.

(118) López Durán, V.; Larsson, P. A.; Wågberg, L. Chemical Modification of Cellulose-Rich Fibres to Clarify the Influence of the Chemical Structure on the Physical and Mechanical Properties of Cellulose Fibres and Thereof Made Sheets. *Carbohydrate Polymers* **2018**, *182*, 1–7. https://doi.org/10.1016/j.carbpol.2017.11.006.

(119) Wang, S.; Oh, J. Y.; Xu, J.; Tran, H.; Bao, Z. Skin-Inspired Electronics: An Emerging Paradigm. *Acc. Chem. Res.* **2018**, *51* (5), 1033–1045. https://doi.org/10.1021/acs.accounts.8b00015.

(120)Tsukada, Y. T.; Tokita, M.; Murata, H.; Hirasawa, Y.; Yodogawa, K.; Iwasaki, Y.; Asai, K.; Shimizu, W.; Kasai, N.; Nakashima, H.; Tsukada, S. Validation of Wearable Textile Electrodes for ECG Monitoring. *Heart Vessels* **2019**, *34* (7), 1203–1211. https://doi.org/10.1007/s00380-019-01347-8.

(121) Isacsson, P.; Jain, K.; Fall, A.; Chauve, V.; Hajian, A.; Granberg, H.; Boiron, L.; Berggren, M.; Håkansson, K.; Edberg, J.; Engquist, I.; Wågberg, L. Production of Energy-Storage Paper Electrodes Using a Pilot-Scale Paper Machine. *J. Mater. Chem. A* **2022**. https://doi.org/10.1039/D2TA04431E.